МІНІСТЕРСТВО ОСВІТИ І НАУКИ УКРАЇНИ
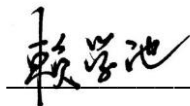## НАЦІОНАЛЬНИЙ АВІАЦІЙНИЙ УНІВЕРСИТЕТ
КАФЕДРА КОНСТРУКЦІЇ ЛІТАЛЬНИХ АПАРАТІВ

ДОПУСТИТИ ДО ЗАХИСТУ
Завідувач кафедри д.т.н, проф.
_____Сергій ІГНАТОВИЧ
«___» _____ 2022 р.

КВАЛІФІКАЦІЙНА РОБОТА
ВИПУСКНИКА ОСВІТНЬОГО СТУПЕНЯ МАГІСТРА
ЗІ СПЕЦІАЛЬНОСТІ
«АВІАЦІЙНА ТА РАКЕТНО-КОСМІЧНА ТЕХНІКА»

Тема: «Дослідження поведінки кобальтового сплаву GH5188 при високотемпературній стискаючій деформації та карта його обробки»

Виконавець:		**Сюечи ЛАЙ**
Керівник: д.т.н., професор	_____	**Михайло КАРУСКЕВИЧ**
Охорона праці: к.т.н., доцент	_____	**Катерина КАЖАН**
Охорона навколишнього середовища:		
к.т.н., професор	_____	**Леся ПАВЛЮХ**
Нормоконтролер: к.т.н., доцент	_____	**Володимир КРАСНОПОЛЬСЬКИЙ**

Київ 2022

MINISTRY OF EDUCATION AND SCIENCE OF UKRAINE

NATIONAL AVIATION UNIVERSITY

DEPARTMENT OF AIRCRAFT DESIGN

<div align="right">

APPROVED BY
Head of department Dr.Sc., prof.
_____ Sergiy IGNATOVICH
"___" _____ 2022

</div>

MASTER DEGREE THESIS
ON SPECIALITY
"AVIATION AND SPACE ROCKET TECHNOLOGY"

Theme: "Study of Hot Compression Deformation Behavior and Processing Map of Cobalt-based superalloy GH5188"

Prepared by:	_____	**Xuechi LAI**
Supervisor: Dr.Sc., professor	_____	**Mykhailo KARUSKEVYCH**
Labor protection:		
Ph.D., associate professor	_____	**Katerina KAZHAN**
Environmental protection:		
Ph.D., professor	_____	**Lesia PAVLIUKH**
Standards Inspector:		
Ph.D., associate professor	_____	**Volodymyr KRASNOPOLSKYI**

Kyiv 2022

НАЦІОНАЛЬНИЙ АВІАЦІЙНИЙ УНІВЕРСИТЕТ

Факультет аерокосмічний
Кафедра конструкції літальних апаратів
Освітній ступінь «Магістр»
Спеціальність 134 «Авіаційна та ракетно-космічна техніка»
Спеціалізації «Обладнання повітряних суден»

ЗАВДАННЯ

на виконання кваліфікаційної роботи пошукача

Сюечи ЛАЙ

1. Тема роботи «Дослідження поведінки кобальтового сплаву GH5188 при високотемпературній стискаючій деформації та карта його обробки», затверджена наказом ректора від 05 жовтня 2022 року №1861/ст.

2. Термін виконання проекту: з 06 жовтня 2022 р. по 30 листопада 2022 р.

3. Вхідні дані до проекту: Енергія термічної активації $Q = 446,1054$ кДж/моль; деформація 0,7, температура деформації близько 1130 °C, швидкість деформації становить близько 1 $с^{-1}$, що є найкращим параметром деформації GH5188;

4. Зміст пояснювальної записки: аналіз стану проблеми, розробка та застосування карти обробки, основні рівняння термічної деформації.

5. Необхідний матеріал: конститутивне рівняння термічної деформації на основі моделі Арреніуса; карта термічної обробки на основі критерію динамічної моделі матеріалів (DMM); аналіз матеріалу за допомогою дифракції зворотного розсіювання електронів (EBSD).

6. Календарний план-графік

№	Завдання	Термін виконання	Відмітка про виконання
1	Огляд робіт стосовно термічної деформації	5.10.2022 – 12.10.2022	
2	Розробка та підготовка випробувань на термічний стиск	13.10.2022 – 14.10.2022	
3	Тест на гаряче стиснення	15.10.2022 – 28.10.2022	
4	Вибір параметрів гарячого стиснення	28.10.2022 – 3.11.2022	
5	Аналіз експериментальних даних, створення моделі процесу	3.11.2022 – 7.11.2022	
6	Охорона праці та навколишнього середовища.	7.11.2022 – 12.11.2022	
7	Завершення пояснювальної записки і презентації роботи	12.11.2022 – 15.11.2022	

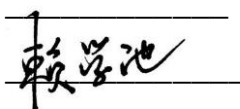7. Консультанти з окремих розділів

Розділ	Консультанти	Дата, підпис	
		Завдання видав	Завдання прийняв
Охорона праці	к.т.н., доцент Катерина КАЖАН		
Охорона навколишнього середовища	к.т.н., профессор Леся ПАВЛЮХ		

8. Дата видачі завдання: 05 жовтня 2022 р.

Керівник дипломної роботи   _____   Михайло КАРУСКЕВИЧ

Завдання прийняв до виконання   _____   Сюечи ЛАЙ

NATIONAL AVIATION UNIVERSITY

Aerospace faculty
Department of Aircraft Design
Educational degree "Master"
Specialty 134 "Aviation and space rocket technology"
Educational professional program "Aircraft equipment"

<div align="right">

APPROVED BY
Head of department Dr.Sc., prof.
_____ Sergiy IGNATOVICH
"___" _____2022

</div>

TASK

For the master degree thesis

Xuechi LAI

1. Topic "Study of Hot Compression Deformation Behavior and Processing Map of Cobalt-based superalloy GH5188" approved by the Rector's order № 1861/ст from 05 October 2022 year.

2. Period of work execution: from 05 October 2022 year to 30 November 2022 year.

3. Initial data: Thermal deformation activation energy Q is 446.1054KJ/mol; Strain is 0.7, the deformation temperature is about 1130℃, Strain rate is about $1s^{-1}$, which is the best deformation parameter of GH5188；

4. Content: State of the art analysis, Development and application of processing map, Thermal Deformation Constitutive Equations.

5. Required material: Thermal deformation constitutive equation based on Arrhenius model; thermal processing map based on Dynamic materials model (DMM) criterion; material analysis by electron backscatter diffraction (EBSD).

6. Thesis schedule

№	Task	Time limits	Done
1	Overview of research on thermal deformation behavior	6.10.2022 – 12.10.2022	
2	Design and prepare thermal compression tests	13.10.2022 – 14.10.2022	
3	Complete the hot compression test	15.10.2022 – 28.10.2022	
4	Select the hot compression data and organize it	28.10.2022 – 3.11.2022	
5	Analyze the data and calculate the model.	3.11.2022 – 7.11.2022	
6	Labor protection and Environmental protection.	7.11.2022 – 12.11.2022	
7	Completion of the explanatory note and PowerPoint presentation	12.11.2022 – 15.11.2022	

7. Special chapter consultants

Chapter	Adviser	Date, signature	
		Task issued	Task received
Labor protection	PhD, associate professor Katerina KAZHAN		
Environmental protection	PhD, professor Lesya PAVLYUKH		

8. Date of issue of the task: 8 September 2022 year.

8. Supervisor: _____ Mykhailo KARUSKEVYCH

Student: _____ Xuechi LAI

РЕФЕРАТ

Пояснювальна записка дипломної роботи магістра «Дослідження поведінки кобальтового сплаву GH5188 при високотемпературній стискаючій деформації та карта його обробки»:

66 сторінок, 39 рисунків, 9 таблиць, 82 літературних посилань

Магістерська робота присвячена проблемі дослідження процесу кування хомутів в системі авіаційних трубопроводів. Вибраний матеріал – GH5188, обговорюється поведінка гарячої деформації та поведінка еволюції мікроструктури цього матеріалу під час кування.

Новизна результатів полягає в досягненні мети контролю еволюції мікроструктури GH5188 і вибору оптимальних параметрів обробки.

Актуальність дослідження обумовлена проблемами високого опору деформації та вузького інтервалу температур обробки в процесі гарячої обробки суперсплавів на основі кобальту.

Методи, що використовуються для отримання результатів: випробування на гаряче стиснення; карта термічної обробки на основі динамічної моделі матеріалу; метод аналізу дифракції зворотного розсіювання електронів (EBSD).

Вищенаведене дослідження показує, що: у поєднанні з картою термічної обробки та аналізом карти EBSD прийнятні параметри термічної деформації сплаву GH5188 визначаються як: температура обробки становить 1080 ℃ ~ 1180 ℃, а швидкість деформації становить 0,1 с-1 ~ 1 с- 1.

Результати дослідження можуть бути використані в авіаційній промисловості, а також у науково-дослідній діяльності.

Деформація гарячого стиснення, суперсплав на основі кобальту, карта обробки, процес кування, система трубопроводів, мікроструктура

ABSTRACT

Master degree thesis "Study of Hot Compression Deformation Behavior and Processing Map of Cobalt-based superalloy GH5188"

66 p., 39 fig., 9 tables, 82 references

Master's thesis deals with the problem of Research on forging process of clamps in aviation piping system. The selected material is GH5188, and the hot deformation behavior and microstructure evolution behavior of this material during forging are discussed.

Novelty of the results is about can achieve the purpose of controlling the microstructure evolution of GH5188 and selecting the optimal processing parameters.

Actuality of the research caused by the problems of high deformation resistance and narrow processing temperature range in the hot working process of cobalt-based superalloys.

Methods used to gain results are hot compression test; Thermal processing map based on dynamic material model; Electron Backscattered Diffraction (EBSD) analysis method.

The above research shows that: Combined with thermal processing map and EBSD map analysis, the reasonable thermal deformation parameters of GH5188 alloy are determined as:The processing temperature is $1080℃\sim1180℃$, and the strain rate is $0.1s^{-1}\sim1s^{-1}$.

Results of the research can be used in aviation industry as well as in research and development activity.

Hot compression deformation, cobalt-based superalloy, processing map, forging process, piping system, microstructure

CONTENT

INTRODUCTION

In this paper, based on the forging process of clamp for aviation piping system, the principle of microstructure change process of superalloy during hot working is explored.

Based on the experimental data obtained from the hot compression processing of GH5188 superalloy, the processing map and the constitutive equation of the hot deformation behavior were established, and the internal microstructure changes during the process were analyzed. The effects of deformation temperature, deformation rate and deformation amount on the high temperature hot deformation behavior of cobalt-based superalloy GH5188 were studied.

PART 1. THE BACKGROUND OF RESEARCH ON THE PIPE CLAMPS FORGING PROCESS OF COBALT-BASED SUPERALLOYl GH5188

1.1 Description of the problem

The development level of the aviation industry, as one of the important indicators of national scientific and technological development and military strength, has always been the focus of research by researchers around the world.Due to the advancement and development of science and technology, the thrust-to-weight ratio required by modern aero-engines is increasing, which puts forward higher requirements for the high-temperature mechanical properties of the hot-end components of the engine.As the main material of aero-engine and hot-end components, superalloy material accounts for more than 60% of its mass [1]. In order to strengthen national defense construction and the development of the national aviation industry, the research and production of superalloys has become the focus of researchers.

Cobalt-based superalloy [2] is an important metal material for the manufacture of aero-engine and gas turbine hot-end components because of its ability to maintain good thermal corrosion resistance, oxidation resistance and welding performance under high temperature conditions of 730 °C to 1200 °C.Among them are the aviation pipeline systems called "blood vessels" and "trachea" of aero-engines [3-5].The aviation pipeline system provides an important guarantee for the normal operation of the aeroengine. The pipeline clamp [6] mainly plays the role of fixing the pipeline position and enhancing the connection strength. At the same time, it also has difficulties such as complicated connection, staggered stacking, and harsh working environment. Just as Figure 1.1. In order to ensure the working quality of the pipeline and maintain the normal operation of the aero-engine pipeline, the processing of the pipeline clamp has attracted the attention of scholars from various countries [7-8]. If there are tissue defects, it will not only have a serious threat to the service life of the parts, but also to the flight safety. Therefore, the material used for the pipe clamp should have good high

temperature bearing capacity and organizational properties. In order to achieve this requirement, it is particularly important to reasonably control the internal structure changes during the material processing and forming process, and to select the best process parameters.

Figure 1-1 Piping System in a modern aircraft engine and Pipe Clamp

The processing properties of superalloys during hot deformation are affected by various process parameters. At present, the main factors that affect the processing performance of materials generally recognized by the academic community are: the inherent properties of the material, the stress state, the initial test structure, the number of processing times, the deformation temperature, the strain rate and the degree of deformation [9]. At the same time, there are problems such as high deformation resistance and narrow processing temperature range during the hot working of cobalt-based superalloys. In order to find reasonable thermal processing parameters for cobalt-based superalloy materials, and to obtain excellent microstructure and properties. The establishment and innovation of thermal processing map technology theory [10-11], which has the advantages of short cycle, low cost and high accuracy, makes this problem effectively solved.Combined with the stress-strain test data obtained in tension or compression, the thermal processing map is a contour plot drawn with T and $\dot{\varepsilon}$ as the coordinate axes to show the processing conditions in the stable and unstable regions of plastic deformation of the material .It can faithfully reflect the internal structure change mechanism of the material during deformation under various deformation temperatures and strain rates according to the actual deformation situation. And the

machinability of the material can be evaluated, and the thermal processing map is of great significance to determine the thermal processing parameters of the material.

On the other hand, in order to more conveniently guide the actual production and reduce the production cost by optimizing the forming process parameters, scholars from various countries [12-13] established the constitutive equations of many materials [14].The constitutive equation expresses the constitutive relationship between the flow stress and strain of a material in the form of a mathematical equation.It can be said that the constitutive relation can reflect the influence of process parameters and microstructure evolution on the flow stress during the deformation process of the material, and can reflect the deformation characteristics of the material.In summary, based on the hot compression test data, the constitutive equations and thermal processing diagrams of the flow stress and strain of cobalt-based superalloy GH5188 are established.The research on the changes in the hot forming process of the clamp made of GH5188 superalloy, and the determination of its hot processing parameters has a certain guiding role.

1.2 Development status at home and abroad

1.2.1 Introduction of GH5188 superalloy

Superalloy refers to high alloyed metal materials with good mechanical properties above 600 °C and certain oxidation resistance. There are many types to meet different service requirements.The first high-temperature alloy was developed by Mond Nickel Company in the United Kingdom.In 1932, British and American scholars Merica et al [15] successfully developed Nimonic75, a nickel-based alloy with creep strengthening effect, on the basis of 80Ni-20Cr electrothermal aluminum alloy by adding a small amount of Ti and C.Subsequently, the company innovatively added B, Zr, Co and other alloying elements, and developed a series of Nimonic alloys [16-17]. Among them, Nimonic80 strengthened by Al and Ti has been successfully used to manufacture the blades of jet turbine engine.In 1942, the American Cobalt Company developed the HastelloyB nickel-based superalloy, and

in 1950, P&W and other companies successfully developed alloy series such as Inconel, Mar-M and Udimet.The development process of superalloys in China is relatively late. China officially started to develop them in 1956, and the first superalloy GH3030 was successfully used in the manufacture of bazooka.Until 1970, the development of superalloys in China had begun to take shape, and a series of superalloys such as GH4037, GH3044, GH4049, GH3128, and K417 were successfully developed [18].

After years of research and exploration, the current research on superalloys in my country can basically meet the needs of China's aero-engine development and production, and more than 100 superalloys have been successfully developed. In the early 20th century, in order to meet the production needs of piston aero-engine turbochargers, high-temperature structural materials with higher temperature resistance were developed, and the research on cobalt-based superalloys gradually attracted people's attention. Compared with traditional nickel-based superalloys, cobalt-based superalloys have become the main materials for manufacturing aero-engine and gas turbine blades due to their superior heat resistance, better thermal corrosion resistance and oxidation resistance in high temperature environments. Cobalt-based superalloys mainly use carbides as the main strengthening item, and a class of alloys with highly alloyed face-centered cubic cobalt-based solid solutions as the matrix, and the cobalt content is about 40%~65% [19]. GH5188 is a cobalt-based superalloy, which can be processed into key components of aero-engines and gas turbines by forging, rolling and other processes. In the process of thermal processing, the organization will produce defects, such as: voids and cracks, which affect the performance of the material after processing. Therefore, the research on thermal deformation and processing parameters of alloys during hot deformation has always been the focus of researchers.

1.2.2 Overview of research on thermal deformation behavior

As an important indicator for judging the deformation treatment of workpieces such as forging, rolling, extrusion, etc., the processing performance of

materials is an important factor to prevent defects such as cracks in the hot working process. At the same time, the structure and mechanical properties of the workpiece are also affected by the thermal processing conditions to varying degrees. Usually, the processing deformation of metal materials above the recrystallization temperature is called thermal deformation. Generally speaking, cold and hot working deformation is not distinguished by the deformation temperature, but is judged according to the recrystallization temperature of the material at a certain deformation rate. After the workpiece is thermally deformed, defects such as pores and defects will be eliminated; In addition, the columnar crystals and dendrites will be refined to produce uniform and fine equiaxed crystals, so that the structure and properties of the material can be improved, and the plasticity and toughness can be improved. In the process of thermal deformation, fibrous tissue will be formed along the direction of tissue deformation, and the mechanical properties of the metal in the direction of tissue deformation are anisotropic, with high mechanical properties.

Therefore, in the thermal deformation process, the performance of the workpiece can be improved by adjusting the deformation temperature, deformation rate and deformation amount. The earliest studies on thermal deformation behavior were conducted by Sellars and Mctegart [20], which proved that flow stress is not only affected by material properties, but also related to thermal processing parameters. Therefore, the processing properties of superalloys during hot deformation are affected by a variety of parameters, mainly including the following two factors: one is the processing technology factors, such as stress state, deformation temperature and strain rate; The second is the inherent properties of the material,Such as the initial structure and ductility of the material. This leads to the complexity of the thermal deformation process of the material, the work hardening and softening mechanisms are affected by deformation parameters, and the deformation conditions directly affect the final metallographic structure. Therefore, it is of great scientific value to analyze the influence law between thermal deformation parameters and flow stress of cobalt-based superalloys, and to

determine the deformation mechanism of plastic deformation of alloys.

Foreign scholars have done a lot of research on the hot deformation mechanism of superalloys. Wang Tao [21] and other scholars calculated the dynamic recrystallization volume fraction of GH4049 superalloy under different thermal deformation conditions based on the true stress-true strain curve data obtained by isothermal compression.And the Avrami model of the dynamic recrystallization volume fraction of the alloy was established, and the proportion of dynamic recrystallization was predicted.

Wang Yan [22] and other scholars used thermal simulation and other research methods to study the slow deformation of as-cast superalloys at high deformation temperature and low strain rate, which is conducive to atomic diffusion and grain boundary migration.Jiang He et al. [23] found that under the same initial forging temperature, too low final forging temperature would inhibit the recrystallization process during hot deformation of GH4738 superalloy.This results in a significant increase in deformation resistance, which affects the structural homogeneity of the alloy. Wilhelm [24] et al. simulated the mechanical fatigue behavior of two single-crystal Ni-based superalloys during hot deformation in the temperature range of 400°C to 980°C. The results show that properly reducing the effective stress has a certain effect on the plastic deformation of the superalloy, and the experiment verifies the accuracy of the simulation well. Abdallah [25] et al. constructed a model based on mathematics and artificial intelligence to simulate and predict the rheological behavior of Haynes 214 superalloy during hot deformation.The results show that the M3_JC model performs the best in terms of the accuracy of rheological behavior prediction, And the predicted value of the SC-FIS model based on artificial intelligence shows that the R value is 0.999, the RE range is -0.79 ~ 1.15 %, and the RMSE value is 0.89MPa. It can be seen that in order to study the best thermal processing parameters in the process of thermal deformation and find out the evolution law of the microstructure of the material under different deformation conditions, numerical simulation technology and physical simulation technology have played a crucial role in the process of thermal deformation

research. .

（1）Numerical simulation technology

Numerical simulation technology, as a combination of computer technology and thermal processing technology, enables direct observation of the effects of process parameters in thermal processing on tissue properties. This breakthrough solves the problems of blindness and experience in traditional thermal processing technology research. Numerical simulation technology makes the research of process parameters evidence-based; At the same time, it can also realize the research on the phase transformation mechanism of thermal processing, and conduct an in-depth analysis of the relationship between phase transformation and performance [26]. At present, the more common numerical models mainly include the rigid-plastic and viscous finite element models proposed by Lee et al. and the Dynamic Materials Models (DMM) established by Gegel and Prasad and other scholars based on irreversible thermodynamic theory.The finite element numerical model is to simultaneously observe the microstructure evolution process of the workpiece under the equivalent stress, equivalent strain and deformation temperature.The simulation results are compared with the experimental results of the workpiece to verify the accuracy of the model predictions. Qiu Qian [27] et al. carried out the simulation with Deform-3D finite element software, and analyzed the instability diagram constructed by combining the thermal compression experimental data.The analysis results show that the finite element simulation of SP700 titanium alloy can effectively predict the unstable deformation region and the change of the hot compression process.Jiang[28-29] and other scholars, through numerical simulation technology, found that in the process of hot working deformation of LSHR alloy, defects such as cracks and voids are likely to occur in the parts where the stress is concentrated.Therefore, the numerical simulation technology provides a great help to determine the thermal deformation process parameters of alloy materials.

(2) Physical Simulation Technology

Physical simulation technology is a test method that simplifies some of the

thermal processing conditions by enlarging and reducing the proportion of the workpiece according to the actual processing conditions.Through the combination with the numerical simulation technology, the experimental technology to reveal the research on the thermal processing properties of materials is achieved. Common physical simulation tests [30] are summarized in the following table 1.1:

Table 1.1 - Common physical simulation tests

Name	Test characteristics and engineering significance
Stretching test	Obtain the basic mechanical properties of materials, such as elastic modulus E, Poisson's ratio μ and yield strength R, etc.; understand the failure of materials at high temperatures.
Compression test	The maximum strain value determined by the compression test is not limited by plastic instability, and is larger than the maximum strain value obtained by the actual tensile test, which provides a design basis for parts under compressive load.
Torsion test	It can comprehensively understand the behavior of high plasticity metal materials under shear stress; can measure its strength and plasticity when the material is in a ductile state; sensitively reflect the surface defects of materials.

The research work in this paper is to obtain the true stress-strain data of GH5188 cobalt-based superalloy through hot compression test and carry out research. Many scholars have used physical simulation technology to study other superalloy materials. For example, Wang Wenbin [31] conducted research on 800H superalloy through single-pass hot compression test. The results showed that the deformation energy storage of high strain rate increased with the increase of dislocation density, and the critical temperature of dynamic recrystallization also decreased. Saeed [32] and other scholars studied the thermal deformation, microstructure evolution and dynamic recrystallization (DRX) mechanism of Co-Al-W superalloy during hot compression through hot compression experiments.It was found that under high temperature conditions, γ-γ'Co-based superalloys formed new grains through special discontinuous DRX in three different regions: the original grain boundary, near the MC carbides, and inside the coarser grains. Special DRX was proposed a descriptive model of a phenomenon. It can be seen that physical simulation techniques such as hot compression tests have played a key role in the research on the hot working process and microstructure evolution of

superalloy materials.

1.3 Research status of metal thermal compression deformation behavior and processing map

1.3.1 Development and application of processing map

Since the 1980s, scholars have evaluated the processing properties of metal materials and obtained their thermal processing maps according to different material models.Ashby et al. [33] studied the effect of process parameters on the forming process of metal materials and established a corresponding deformation mechanism diagram.However, these deformation mechanism diagrams have many limitations, such as: they are only applicable to low strain rate states and mainly focus on the creep mechanism.

To address the limitations of the Ashby machining map, Raj et al. [34] comprehensively considered the effects of deformation temperature and strain rate on the machining properties of metal materials, And according to the atomistic model (Atomistic Model), the safety diagram is established on the premise that there is no unstable state in the metal material. However, this safety map also has many shortcomings, such as the parameters required to construct the map are extremely difficult to obtain; for complex alloys, the map is not applicable; This figure can only give the safe process parameters of metal material forming, and cannot realize the optimization of parameters. Based on previous research results, Prasad et al. [35] proposed Dynamic Material Modeling, or DMM model. In the DMM model, the workpiece is regarded as a nonlinear power dissipator, and the entire deformation process can be regarded as an energy dissipation system affected by the rheological behavior of the metallic material [36]. Many subsequent scholars [37-41] further improved the dynamic material model, and finally drew the power dissipation diagram and the instability diagram based on different instability criteria.The DMM-based thermal process map is obtained by superimposing these two graphics.

1.3.2 Establishment and application of constitutive equations

The relationship between flow stress and deformation temperature, deformation degree, and strain rate during the deformation process of the material is called the mechanical constitutive relationship, which is the dynamic response between the thermal parameters of the material during the high temperature plastic deformation process. At present, there are mainly statistical constitutive models and phenomenological constitutive models. The former is based on the microscopic angle to describe the microstructure evolution of the material when it is deformed at high temperature; The latter is based on phenomenological theory, and the constitutive relation established by nonlinear fitting of experimental results based on mathematical statistics or artificial neural network. This model is widely used in engineering [42]. For example, Lei Jinwen [43] et al. established a constitutive model of Ti6242s alloy based on the thermal compression simulation test data, and predicted the flow stress under the deformation parameters of the deformation temperature of 950 °C.The results show that the correlation coefficient R is 0.99905 and the average relative error AARE is 1.93%, indicating that the constitutive model has good generalization ability and can predict the flow stress of other test parameters.Kim [44] et al. constructed an artificial neural network for high temperature oxidation performance analysis of Ni-based superalloys composed of Ni-Co-Cr-Mo with alloy content as input and mass gain as output.And determined the element ratio with the best anti-oxidation performance at high temperature.

Palavar [45] et al. established a neural network model to predict the relationship between aging parameters and wear behavior of IN706 superalloy.The results show that by observing the test results of different aging, it can be clearly seen that δ, γ' and γ" phases appear near the grain boundaries of IN706 alloy, and the test shows that the sample with the highest hardness is aged for 12h,It is basically consistent with the prediction result of artificial neural network. The artificial neural network has obtained a series of research results in the research of metal materials, but its macroscopicity is still relatively weak in showing the

changes in the microstructure of materials. The constitutive model of the physical concept can gradually add microphysical variables such as grain size and dislocation density into the constitutive equation, which has a greater advantage in describing the evolution of the microstructure. Considering the influence of slip on plastic deformation and the difference of Taylor factor of twinning region, the evolution of dislocation density and twinning integral fraction is considered. Sun Chaoyang [46] et al. established a plastic physical constitutive model for the slip and twinning of Fe-22Mn-0.6C twin-induced plasticity (TWIP) steel. It is proved that the slip rate is negatively correlated with the slip rate, which better reflects the interaction of twinning and slip mechanism. Su Jing [47] et al. established a physical constitutive model of cast magnesium alloy AZ31 based on the thermally activated dislocation mechanism.The model can better predict the plastic flow stress of the alloy at high stress-strain rates and different temperatures, and the prediction effect is good.Wang Jun [48] cited a physical constitutive model considering the influence of deformation temperature on self-diffusion coefficient and elastic modulus in the study of NiTi shape memory alloy, which has certain guiding significance for optimizing the hot forming process parameters of the alloy. Composite materials are easily affected by many factors in the process of high temperature plastic deformation, and their high temperature plastic rheological behavior is extremely complex.There are various deformation mechanisms in the high temperature plastic deformation process of composite materials, which makes the high temperature rheological mechanical behavior extremely complex.The phenomenological constitutive model is the most widely used model in the establishment of the thermal deformation constitutive relationship of most metal materials. The constitutive model can describe the relationship between flow stress, deformation parameters and deformation amount from a macro perspective. Common phenomenological constitutive models include: Johnson-Cook model [49] Arrhenius model [50] and Fields-Backofen model [51].The J-C model is used as a phenomenological constitutive model to describe the deformation behavior of materials at high deformation temperature and high deformation rate.It takes into

account the strain strengthening term and thermal softening term, and forms the mathematical expression as follows:

$$\sigma = \left(A + B\varepsilon^n\right)\left[1 + C\ln\left(\dot{\varepsilon}/\dot{\varepsilon}_0\right)\right]\left[1 - \left(\frac{T - T_{ref}}{T_m - T_{ref}}\right)^m\right] \tag{1.1}$$

among, $\left(A + B\varepsilon^n\right)$ represents the strain hardening term,

$\left[1 + C\ln\left(\dot{\varepsilon}/\dot{\varepsilon}_0\right)\right]$ represents the strain rate hardening term,

$$\left[1 - \left(\frac{T - T_{ref}}{T_m - T_{ref}}\right)^m\right]$$ represents the thermal softening term.

Lin [52] et al. compared the experimental data of Al-Cu-Mg alloy with the stress value curve predicted by the J-C model, and found that under some parameters, there was a significant deviation between the predicted value and the experimental value.This is because the coupling effect between strain, strain rate and deformation temperature is ignored in the J-C constitutive model, and the strain hardening term is considered separately.

Physical models can more accurately describe the deformation behavior of materials at different temperatures and strain rates. For example, the Arrhenius model can be established to accurately characterize the flow behavior of materials, and the Arrhenius model is a typical research object based on the change trend of the flow stress curve, and its application in materials is very wide [53-56].*Jonas and Sellars* [57] considered the deformation activation energy Q, and the expression is shown in (1-2); at the same time, the ***Zener-Hollomon*** parameter [58] (Z parameter) was introduced, which creatively made up for the failure to consider the J-C constitutive model. Coupling of temperature, s59train rate and flow stress. The practicability of the constitutive equation based on Arrhenius equation has been proved in many studies.

$$Q = R\left[\frac{\partial\ln\dot{\varepsilon}}{\partial\ln\left[\sinh\left(\alpha\sigma\right)\right]}\right]_T\left[\frac{\partial\ln\left[\sinh\left(\alpha\sigma\right)\right]}{\partial\left(1/T\right)}\right]_{\dot{\varepsilon}} \tag{1.2}$$

It is worth noting that for materials with dynamic recrystallization behavior in the

microscopic deformation mechanism, σ is generally selected as the peak stress σ_p [59].

1.4 Conclusion

1. This paper mainly introduces the application of superalloys in the aviation industry, especially the development process of cobalt-based superalloys, by summarizing and summarizing related papers;

2. The research progress of hot deformation behavior of superalloy materials is basically described, and the research methods of hot deformation behavior such as hot working diagram and constitutive equation are introduced.

PART 2. DESIGN OF RESEARCH METHOD FOR GH5188 SUPERALLOY MATERIAL

The purpose of this section is to design thermal compression experiments and to establish thermal processing maps for GH5188.The thermal deformation behavior of GH5188 superalloy in the forging process is studied, and the process of the clamp of aviation pipe fittings is simulated.The results of the hot compression experiment can provide the true stress-strain experimental data of the GH5188 superalloy, and provide parameters for the establishment of the hot working map.

2.1 Experimental scheme of thermal compression

2.1.1 Experimental materials and sample preparation

GH5188 alloy is a solid solution strengthened cobalt-based superalloy with carbide as the main strengthening phase.It has stronger thermal corrosion resistance, thermal fatigue resistance, and high temperature strength than nickel-based superalloys [60]. It has obvious advantages in manufacturing some high-temperature parts of aero-engines. In order to control the microstructure evolution of GH5188 and select the best processing parameters, this chapter is based on the hot compression experiment to obtain the true stress-strain curve of GH5188 during the forging process.At the same time, the microstructure of the hot-compressed sample was observed and the thermal deformation behavior was studied in combination with the thermal processing map.Referring to the high-temperature plasticity diagram of GH5188 alloy [61], in order to reduce the deformation resistance and filling difficulty of the metal during processing, the final forging temperature of GH5188 superalloy should not be lower than 980°C, as shown in Figure 2.1.
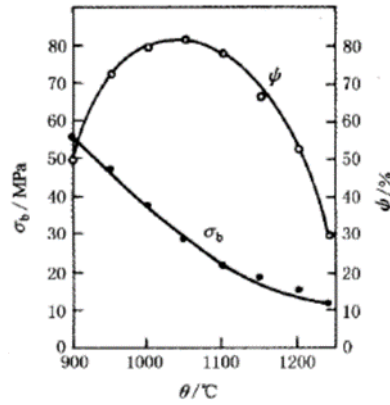
Figure 2.1 - High temperature plasticity diagram of GH5188 alloy

The material selected in this test is a rod-shaped ingot of GH5188 alloy that has undergone solid solution strengthening treatment, and its specific chemical composition is shown in Table 2.1.The original microstructure map and scanning electron microscope (SEM) microstructure of GH5188 are shown in Figure 2.2. It can be seen from Figure 2-2 that M_6C and $M_{23}C_6$ carbides are precipitated inside the grains and on the grain boundaries, and the grain size is about 16 μm.

Table 2.1 - GH5188 alloy composition range

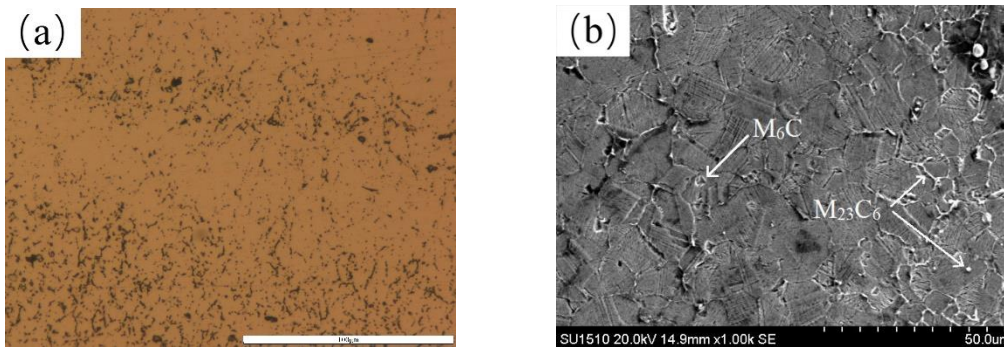| Element	C	Cr	Ni	W	Fe	Mn	Si	La	Co
Content（wt.%）	0.1	20.0~24.0	20.0~24.0	13.0~16.0	≤3.0	≤1.25	≤0.20	0.1	Margin

Figure 2.2 - The original microstructure of GH5188 alloy (a) and SEM microstructure (b)

2.1.2 Experimental scheme of thermal compression

In this paper, the rheological behavior and dynamic recrystallization behavior of GH5188 superalloy are studied by single-pass hot compression test. The test flow is shown in Figures 2.3 and Figures 2.4. On the uniformly treated GH5188 sample, several hot-compressed cylindrical samples with a size of Φ10mm × 15mm were cut by a wire cutting machine, as shown in Figure 2.5. In order to

reduce the influence of friction on subsequent tests, both ends of the sample were polished with sandpaper and covered with tantalum sheets, and both ends were lubricated with MoS2 powder, and then the thermocouple was welded on the surface of the sample.In this test, the Gleeble-1500 thermal/mechanical simulation test equipment was used to conduct the isothermal constant strain rate thermal compression test.First, the temperature was raised to the holding temperature at a heating rate of 20°C/s, and held for 180s to keep the samples in each group in a consistent state. Then cool down, slowly reach the deformation temperature of the sample, and perform a compression test at the same temperature after holding for 30 s.Immediately after compression, water quenching is performed to preserve the deformed microstructure. In order to achieve a good prediction effect, the test temperature is selected within the temperature range during the forging process.
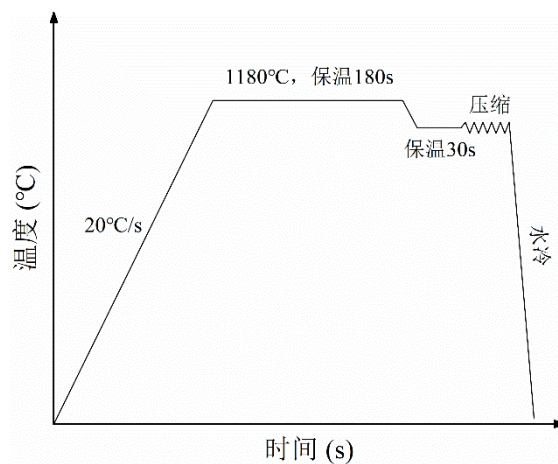

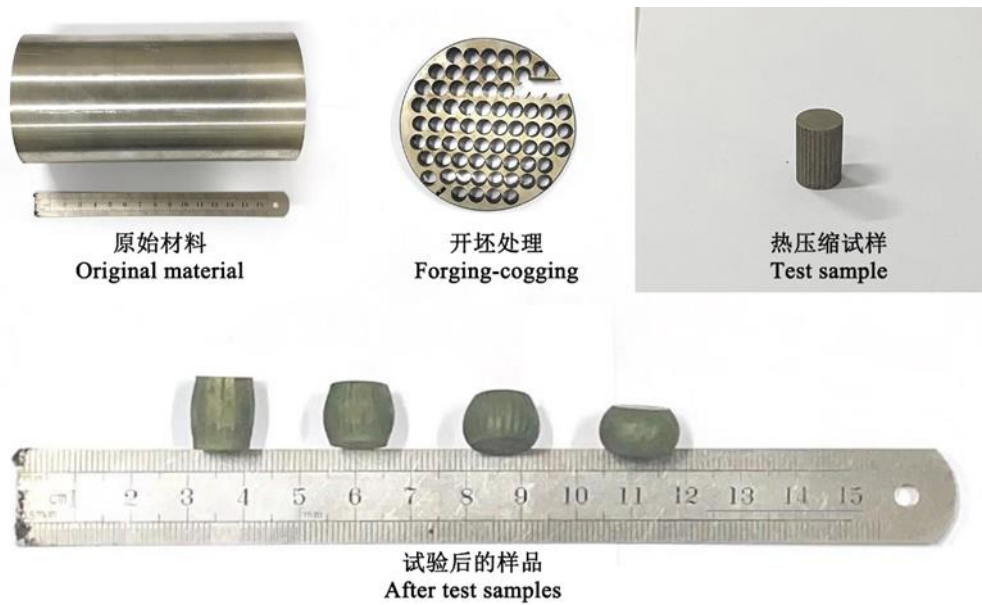Figure 2.3 - Compression test flow chart

原始材料
Original material

开坯处理
Forging-cogging

热压缩试样
Test sample

试验后的样品
After test samples

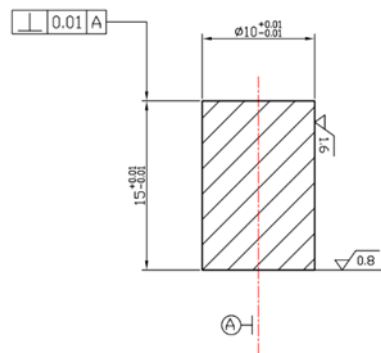Figure 2.4 - GH5188 alloy material processing flow chart

Figure 2.5 - Compression Specimen Dimensions

2.2 Electron Backscattered Diffraction（EBSD） detection scheme

In order to characterize the microstructure evolution process of GH5188 alloy during hot compression, it is necessary to observe and analyze the samples after hot deformation. EBSD technology uses electron beams to generate diffraction on the lattice plane of the crystal. According to the difference of the diffraction pattern in different crystal directions, the distribution map of the atomic arrangement in the observation area is obtained. In this experiment, the ZEISS MERLIN Compact field emission scanning electron microscope (Figure 2.6) produced by JEOL Co., Ltd. was used. Obtain the crystal orientation information of the sample through the

EBSD accessory, and observe the recrystallization characteristic structure of the sample. In the process of EBSD data analysis, the AZtecHKL CHANNEL5 software was used to process the images using the Brandon criterion, to distinguish the recrystallized structure and the deformed structure according to the average grain orientation difference, and to determine the recrystallized fraction information of the microstructure.And obtained the grain orientation map, pole figure and reverse pole figure including band contrast information (BC), grain boundary composition information (GB) and recrystallization fraction information (RF).According to the recrystallized grain morphology and grain internal orientation information, the recrystallization mechanism during hot deformation of GH5188 alloy was deduced.

Figure 2.6 - ZEISS MERLIN Compact Field Emission Scanning Electron Microscope

In the hot compression test, due to the friction between the upper and lower surfaces of the sample and the loading platform, the material flow on the contact surface is blocked, and the overall stress of the sample is not completely consistent.According to the three-dimensional force conditions of the sample, it can be divided into three regions, as shown in Figure 2.7. Zone I is the difficult deformation zone, zone II is the easy deformation zone, and zone III is the small deformation zone.In this paper, the easily deformable area in the center of the sample is taken, and the EBSD observation position in this paper is taken from the center of the easily deformable area. The thermally compressed sample is cut radially from the center, and then a sample with a size of 7mm*7mm*2mm is cut

by wire cutting. EBSD technology requires the surface of the sample to be clean, free of oxidation, and flat, so it is necessary to grind and polish the wire-cut sample.Use 400-mesh, 800-mesh, 1000-mesh, and 1500-mesh sandpaper to grind the surface of the inlaid sample in turn, and polish it with Cr2O3 powder on a polishing machine.Due to the stress on the surface of the sample during the polishing process, the sample needs to be electropolished, that is, polished with a DC voltage of 10V in the electrolyte (nitric acid:methanol=3:7) for about 30s.And use liquid nitrogen to cool the sample, keep it at about -30 ℃, and clean the surface with alcohol immediately after polishing.The acceleration voltage of the SEM was set to 30KV, and different scanning step sizes (0.3 μm, 0.55 μm) were selected according to the grain size to speed up the detection speed while ensuring the scanning quality. By calibrating the orientation of different grains, recrystallized grains and unrecrystallized grains are distinguished, the recrystallization mode of GH5188 superalloy is determined, and the recrystallization fraction and recrystallized grain size are accurately calculated.
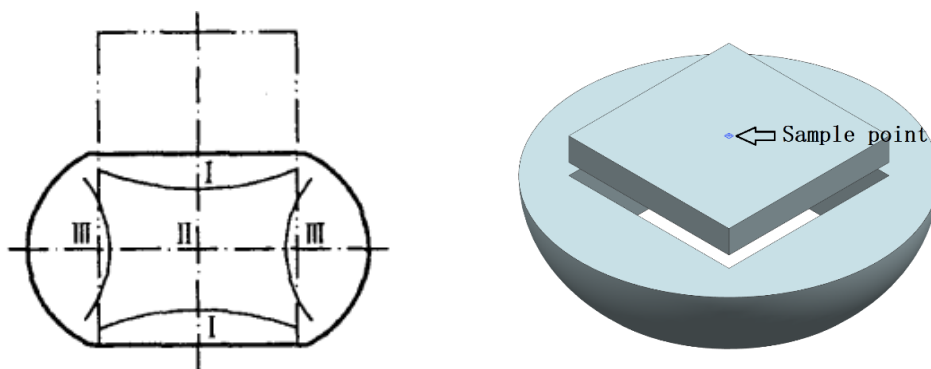
（a）Compression Deformation Partition   （b）EBSD sample observation point
Figure 2.7 - Division of thermal compression deformation area (a) and sampling (b)

2.3 Theory of thermal processing map

In order to prevent defects in the material during deformation, such as adiabatic shear bands, coarse grains, grain boundary defects, etc., Prasad et al. [62] based on the dynamic materials model (DMM).A conceptual approach to thermal processing maps is established based on mechanics, thermodynamics, and physical system theories.In the dynamic material model, the deformation process is

regarded as a consumption process of energy (P), and there are two main consumption paths: heat dissipation (G) and dissipation caused by tissue evolution (J).The relationship between these three variables is:

$$P=G+J=\int_0^{\dot{\varepsilon}} \sigma d\dot{\varepsilon}+\int_0^{\sigma} \dot{\varepsilon} d\sigma \qquad （2.1）$$

And the dissipation efficiency factor η is introduced to measure the proportion of the total dissipated energy occupied by the tissue evolution during the deformation process, which is expressed as:

$$\eta=\frac{J}{J_{max}} \qquad （2.2）$$

Among them, is the maximum tissue dissipation value under ideal conditions, which can generally be taken as P/2. And the strain rate sensitivity coefficient m is introduced, which reflects the ratio between the energy of the two dissipation modes. The definition formula is:

$$m=\left(\frac{\partial J}{\partial G}\right)_{T,\varepsilon}=\frac{\partial \ln \sigma}{\partial \ln \dot{\varepsilon}} \qquad （2.3）$$

Under a certain deformation condition, the constitutive equation of stress to strain rate can be simply expressed as:

$$\sigma=k\varepsilon^m \qquad （2.4）$$

Substituting it into Equation (2.2) and Equation (2.3), the expression of the dissipation efficiency factor can be obtained as:

$$\eta=\frac{2m}{m+1} \qquad （2.5）$$

The larger the value of η, the larger the proportion of energy consumed by the microstructure evolution during the deformation process, that is, the higher the recrystallization volume fraction.During the compression process of the material, when the load reaches a certain critical value, severe plastic deformation will occur, resulting in the material being in an unstable state, manifested as local plastic flow, the formation of adiabatic shear bands, cavity nucleation and cracking etc.This phenomenon is called plastic instability.Prasad [64] proposed a criterion for judging plastic instability based on the principle of maximum entropy generation rate:

$$\xi(\dot{\varepsilon})=\frac{\partial\ln[m/(m+1)]}{\partial\ln\dot{\varepsilon}}+m<0 \qquad\qquad （2.6）$$

When $\xi(\dot{\varepsilon})$ is less than 0, it means that plastic instability may occur under this deformation parameter, and this range should be avoided when selecting processing parameters. The superposition of the power dissipation diagram and the plastic instability diagram can not only reflect the microstructure evolution law of the material but also avoid the plastic instability region, forming a comprehensive thermal processing diagram. According to the thermal processing map, not only can reasonable process parameters be selected, the generation of forging defects can be avoided, and the structure of the material after processing can be improved. Moreover, the ideal organizational structure can be obtained by controlling the process parameters, which has certain guiding significance for the selection and formulation of process parameters.

2.4 Conclusion:

This part takes GH5188 superalloy as the experimental material, and designs the single-pass hot compression experiment in detail.And according to the test, the raw materials of GH5188 were processed and cut, and the test samples that met the test requirements were prepared. The EBSD technology was used to prepare for the analysis of the microscopic characteristics of the deformation structure of the GH5188 superalloy under different process parameters, so as to study the change law of the recrystallized structure;Finally, the principle and establishment idea of thermal processing map are introduced.

PART 3. CALCULATION OF CONSTITUTIVE EQUATION AND PROCESS MAP

3.1 Test Results and Analysis

The true stress-true strain curves of GH5188 at different deformation temperatures and strain rates are shown in Figure 3.1 (a-c). It can be seen from Fig. 3.1(a-c) that the shape of the curve is basically the same under all test conditions. When the strain rate is small, the hot compressive flow stress of the GH5188 superalloy increases rapidly first. After the material reaches the yield point, the flow stress continues to increase with the increase of strain, indicating that the strain hardening effect at this stage is greater than the temperature softening effect of the material. After reaching a peak value near the strain of 0.2, it gradually decreases and tends to a stable value, reaching the steady-state flow stress. This indicates that the temperature softening effect is dominant at this stage. By comparing the real stress-true strain curves under different test parameters,it can be found that the decreasing trend is more obvious when the strain rate is $10s^{-1}$. This is in high agreement with the deformation behavior of other cobalt-based superalloys [65]. The thermal deformation process of metal materials is a process in which the softening mechanism and the hardening mechanism interact.In the initial stage of deformation, due to the continuous increase of dislocations, the interaction of dislocations increases the resistance of the dynamic recrystallization process, which in turn leads to work hardening inside the material, thereby increasing the stress.When the deformation reaches a critical value, the dislocation density reaches the critical density required for dynamic recrystallization, and a recrystallization nucleus is formed. The growth process of the recrystallization nucleus and the dislocation balance each other, so that the stress reaches a peak value. In the later stage of deformation, when the proliferation of dislocation density and the reduction of dislocation density caused by dynamic recrystallization reach a dynamic equilibrium, a steady-state rheological
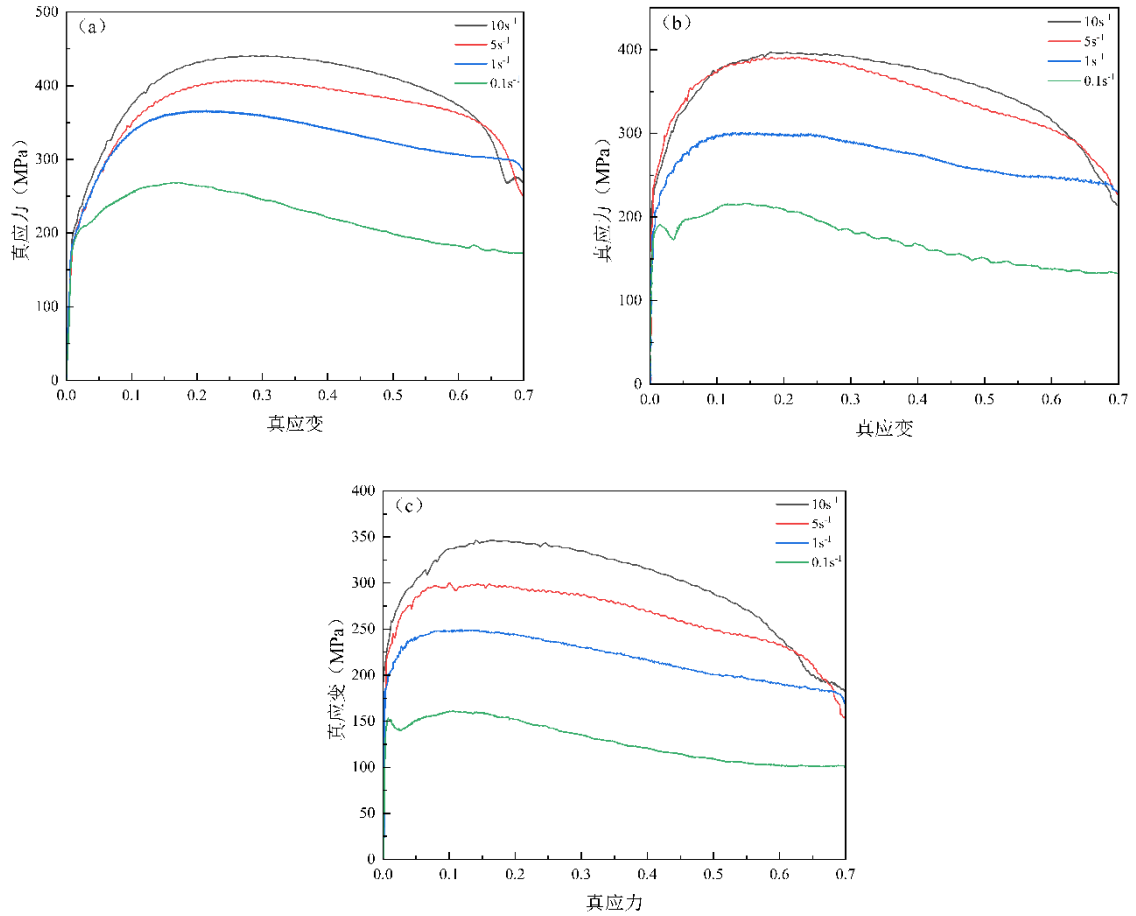
phenomenon occurs in stress.

Fig.3.1 - True stress-true strain curves under different test parameters, (a) 1080℃, (b) 1130℃, (c) 1180℃

Figure 3.2 reflects the dynamic response of peak stress to process parameter changes, and found that GH5188 alloy has lower peak stress at higher temperature and lower strain rate. The slip of dislocations is a thermally activated process. At higher temperatures, the initiation and slip of dislocations are more likely to proceed, and recovery and recrystallization are prone to occur, reducing the dislocation density; When the strain rate increases, because the mechanism of plastic deformation is more complex, and there is not enough time for plastic deformation and softening, it will appear more elastic.
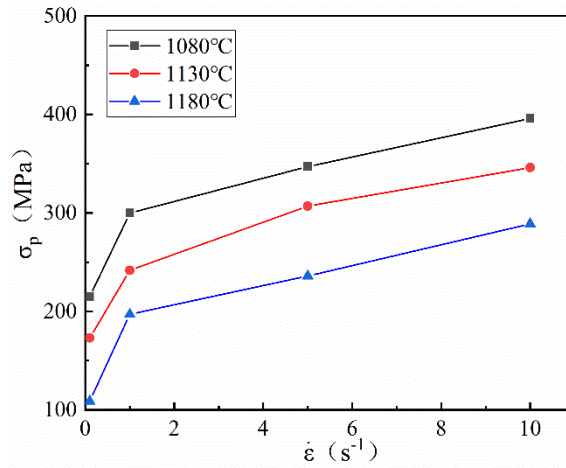
34

Figure 3.2 Peak stress at different strain rates at different temperatures

It is worth noting that the material exhibits obvious recrystallization characteristics under low strain rate conditions, and two peaks appear on the flow stress curve, which is related to the trade-off between deformation rate and recrystallization rate [63]. At high temperature, dynamic recrystallization occurs when the deformation energy is greater than the activation energy of recrystallization, and the large deformed grains are replaced by new grains, and the stress decreases. If the total load remains unchanged, the deformation rate will increase at this time. At this time, the deformation accumulation rate is higher than the recrystallization rate, the material will harden, and the stress will increase. Due to the accumulation of deformation, the recrystallization rate will increase again at this time, which is greater than the rate of accumulation of deformation, and the material softens again. After such a few oscillations, the two automatically find a balance, and the curve becomes stable.

3.2 Establishment of hot deformation constitutive model of GH5188 superalloy

As a mathematical equation describing the macroscopic properties of materials, the material constitutive relation is used to construct the relationship between flow stress and deformation parameters during thermal deformation of materials through mathematical methods.The feasibility of the constitutive model in the study of thermal deformation behavior has been proved both in the actual machining

process and in the existing studies.The thermal deformation process of superalloys is also a thermal activation process, so the Q value of thermal activation energy is an important parameter reflecting the dislocation mechanism and evolution mechanism in thermal deformation.

Taking the change trend of the flow stress curve as the research object, Jonas and Sellars considered the deformation activation energy Q and proposed a constitutive equation based on the Arrhenius equation, which is divided into three forms according to the stress level:

for low stress levels（$\alpha\sigma \leq 0.8$）：

$$\dot{\varepsilon} = A_1 \sigma^{n_1} \exp\left[-Q/(RT)\right] \tag{3.1}$$

for high stress levels（$\alpha\sigma \geq 0.8$）：

$$\dot{\varepsilon} = A_2 \exp(\beta\sigma) \exp\left[-Q/(RT)\right] \tag{3.2}$$

at all stress levels：

$$\dot{\varepsilon} = A_3 \left[\sinh(\alpha\sigma)\right]^n \exp\left[-Q/(RT)\right] \tag{3.3}$$

where Q is the deformation activation energy；；

R is the gas molar constant, and its value is 8.314J/(mol·K)；

A is the structure factor (s-1), independent of temperature；

α, β are temperature-independent stress level parameters and satisfy $\alpha=\beta/n$；

n is the work hardening index, which is used to measure the distribution of strain in the material during thermal deformation.

In order to comprehensively consider the interaction between the deformation temperature and the strain rate, Jonas and Sellars introduced the temperature compensation factor Zener-Hollomon parameter (Z parameter) into their model. As shown in Eq. (3.4), the coupling equation of temperature, strain rate and flow stress can be obtained immediately by combining the two equations.

$$Z = \dot{\varepsilon}\exp(Q/RT) = A_4\sinh^n(\alpha\sigma) \tag{3.4}$$

Taking the logarithm of both sides of equation (3-1), there is

$$\ln\dot{\varepsilon} = n\ln\sigma + \ln A_1 - Q/RT \tag{3.5}$$

Taking the experimental data with a strain of 0.7 as an example, the stress-strain data of GH5188 is processed by the Origin drawing software, and the peak stress under each parameter is obtained, as shown in Table 3.1.

Table 3.1 - Peak stress for different parameters at 0.7 strain

Strain rate ($\dot{\varepsilon}$ /s^{-1})	Peak Stress σ_p		
	1080°C	1130°C	1180°C
0.1	266.83	215.00	160.72
1	364.55	299.35	246.60
5	406.99	390.20	295.46
10	439.51	396.07	345.31

At the same temperature, a scatter plot of **ln$\dot{\varepsilon}$** and **lnσ_p** is established by linear fitting of the experimental data, and then a linear regression analysis is performed on the data points to obtain a straight line as shown in Figure 3.2.
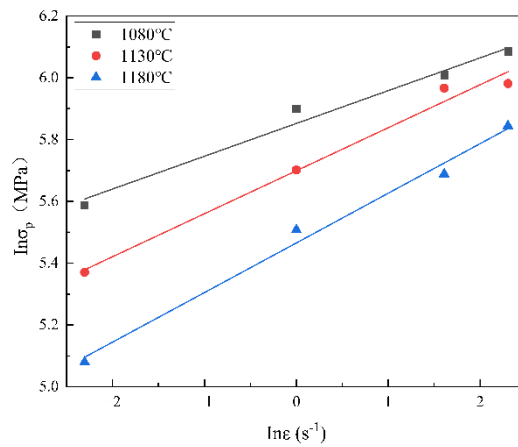

Figure 3.3 Linear fit plot of **ln$\dot{\varepsilon}$** and **lnσ_p**

After sorting out the slope and intercept data of the fitted curve, the following table 3.2 can be obtained:

Table 3.2 Linear fitting parameters of **ln$\dot{\varepsilon}$** and **lnσ_p** at different temperatures

Temperature	Slope	Intercept
1080°C	0.10619	5.85222
1130°C	0.13926	5.69911
1180°C	0.16068	5.46548

Through calculation, the average value of the reciprocal of the slope is n_1, and its value is 7.38716. By taking the logarithm of both sides of equation (3.2) at the same time, the following formula is obtained:

$$\ln\dot{\varepsilon}=\beta\sigma+\ln A_2-Q/RT \qquad (3.6)$$

At the same temperature, by studying the linear relationship between **ln$\dot{\varepsilon}$** and σ, a scatter plot of **ln$\dot{\varepsilon}$** and σ is established, as shown in Figure 3.3 below:
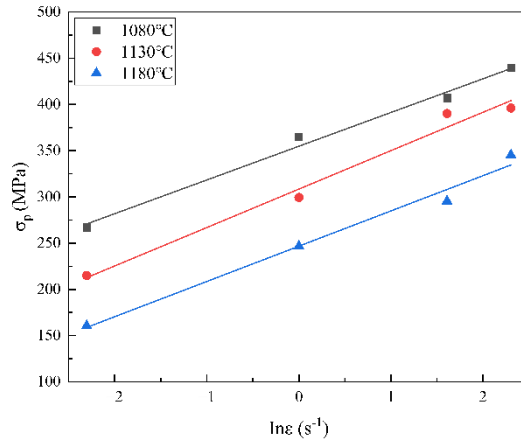
Figure 3.4 - Linear fitting diagram of $\ln\dot{\varepsilon}$ and σ_p

It can be clearly seen from the figure that there is basically a linear relationship between the two. After sorting out the slope and intercept data of the fitting curves of **ln$\dot{\varepsilon}$** and **σ_p**, the following table 3.3 can be obtained:

Table 3.2 - Linear fitting parameters of **ln$\dot{\varepsilon}$** and **σ_p** at different temperatures

Temperature	Slope	Intercept
1080°C	36.5028	354.7886
1130°C	41.5746	308.4285
1180°C	38.1663	246.6735

By calculating the data in the table, the average value of the reciprocal slope is the parameter β in the equation, and its value is 0.025. Further through the formula: α=β/n_1, the value of the constant α can be obtained as 0.0034.

Taking the logarithm of both sides of formula (3.3) and arranging, the following formula can be obtained:

$$\ln\left[\sinh(\alpha\sigma_p)\right] = \frac{1}{n}\ln\dot{\varepsilon} - \frac{1}{n}A_3 + \frac{Q}{n\,RT} \tag{3.7}$$

Then, with $\ln\dot{\varepsilon}$ as the independent variable and $\ln\left[\boldsymbol{sinh(\alpha\sigma_p)}\right]$ as the dependent variable, the relevant values at different temperatures can be obtained by arranging the data, as shown in the following table.

Table 3.4 - $\ln\left[\boldsymbol{sinh(\alpha\sigma_p)}\right]$ values at different temperatures

strain rate （$\dot{\varepsilon}$ /s^{-1}）	ln$\dot{\varepsilon}$	$\ln\left[\sinh(\alpha\sigma_p)\right]$ 1080°C	1130°C	1180°C
0.1	-2.3025	0.0706	-0.1938	-0.5251
1	0	0.4989	0.2208	-0.0282
5	1.6094	0.6687	0.6023	0.2034
10	2.3025	0.7948	0.6256	0.4194

At the same temperature, by studying the linear relationship between ln$\dot{\varepsilon}$ and

38

$\ln[sinh(\alpha\sigma_p)]$, the fitting curve of $\ln\dot\varepsilon$ and $\ln[sinh(\alpha\sigma_p)]$ is established, as shown in Figure 3-4 below:
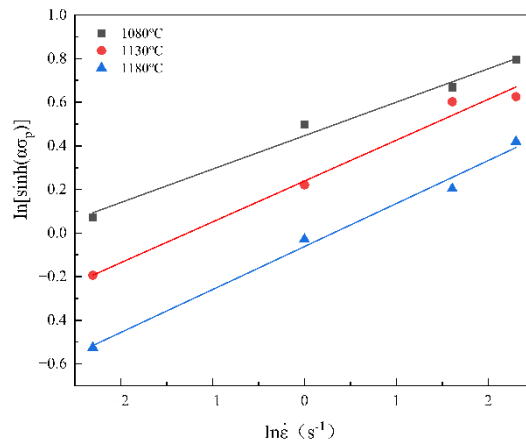

Figure 3.5 - Linear fitting diagram of $\ln\dot\varepsilon$ and $\ln[sinh(\alpha\sigma_p)]$

It can be easily observed that under the three different temperature conditions, all have substantially the same slope. By sorting out the fitting curve results, Table 3-5 can be obtained:

Table 3.5 - Linear fitting parameters of $\ln\dot{\varepsilon}$ and $\ln\left[sinh(\alpha\sigma_p)\right]$ at different temperatures

Temperature	Slope	Intercept
1080°C	0.1534	0.4465
1130°C	0.1874	0.2383
1180°C	0.1972	-0.0612

Take the reciprocal of the slope of the fitting curve at different temperatures, and calculate the average to be n, and the value is 5.5755. Similarly, on the basis of formula (3.7), with $\frac{1}{T}$ as the independent variable and $\ln\left[sinh(\alpha\sigma_p)\right]$ as the dependent variable, $\ln\dot{\varepsilon}$ is regarded as a fixed value at this time. By establishing a scatter plot between the two and performing a linear fit on it, the results are shown in the following figure:
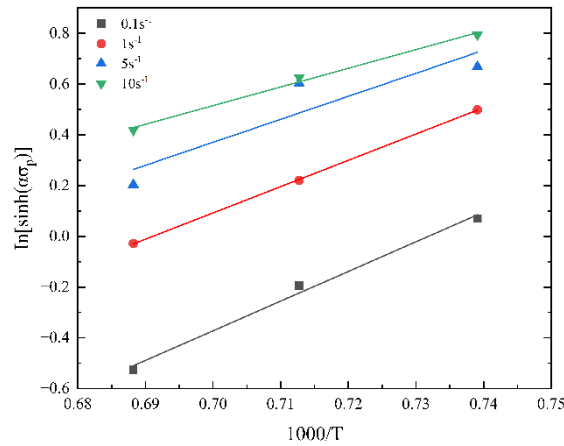

Figure 3.6 - Linear fitting diagram of $\frac{1}{T}$ and $\ln\left[sinh(\alpha\sigma_p)\right]$

By calculating the relevant parameters of the fitting curve, the following table 3.6 is obtained:

Table 3.6 - Linear fitting parameters of $\frac{1}{T}$ and $\ln\left[sinh(\alpha\sigma_p)\right]$ at different temperatures

Strain rate（$\dot{\varepsilon}$ /s^{-1}）	Slope	Intercept
0.1	7.3695	-4.6437
1	9.0681	-5.9772
5	10.3671	-7.1650
10	11.6940	-8.5581

In formula (3.7), let $K=\dfrac{Q}{nR}$, the K value can be calculated to be 9.6247. From this, we can obtain the thermal deformation activation energy $Q=RnK$ of GH5188.

Substitute the corresponding value to obtain the thermal deformation activation energy Q value is **446.1054KJ/mol.** By taking the logarithm of both sides of the expression (3-4) of the temperature compensation factor Z parameter,

it can be obtained:

$$InZ=InA_4+In[sinh^n(\alpha\sigma_p)] \tag{3.8}$$

It can be seen from formula (3.8) that InZ and $In[sinh^n(\alpha\sigma_p)]$ have a linear relationship, and the thermal activation energy Q value calculated above is calculated. And related deformation parameters such as deformation temperature (T) and deformation rate ($\dot{\varepsilon}$) are substituted into formula (3.8) to obtain the corresponding temperature compensation factor Z value.Then the data related to InZ and $In[sinh^n(\alpha\sigma_p)]$ can be obtained, and linear fitting is performed, as shown in Figure (3.6):
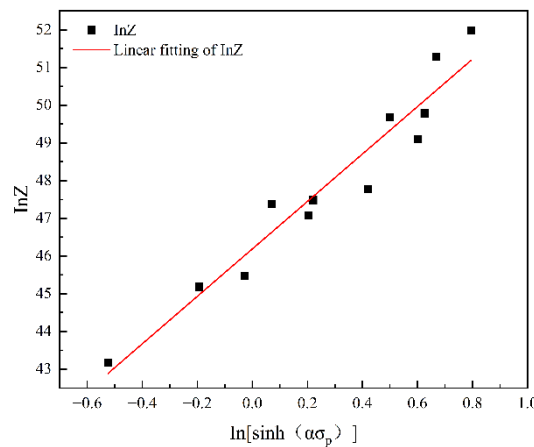

Figure 3.7 Linear fitting diagram of InZ and $In[sinh^n(\alpha\sigma_p)]$

Through the analysis of the fitting results, it is known that the linear regression correlation coefficient R=0.9357.

The relationship between flow stress, deformation temperature and strain rate of GH5188 superalloy during hot compression deformation is well proved.It can be described by the hyperbolic sine function of the Arrhenius-type constitutive model.Based on the above calculation results, the following table 3-7 can be obtained:

Table 3.7 - Related parameters of thermal deformation constitutive equation

A	n_1	A_4	Q
0.0034	7.3872	1.1461×10^{20}	446.1054KJ/mol

Substitute the relevant parameters of the hot deformation constitutive equation in Table 3.7 into formulas (3.3) and (3.4) to obtain the hot deformation

constitutive equation of GH5188 superalloy and the expressions of flow stress and Z parameters as follows:

$$\dot{\varepsilon}=1.1461\times10^{20}\left[\sinh(0.0034\sigma)\right]^{7.3872}\exp\frac{\left[-44610.5\right]}{RT} \tag{3.9}$$

$$\sigma=(\frac{1}{0.0034})\ln\left\{(\frac{Z}{1.1461\times10^{20}})^{\frac{1}{7.3872}}+[(\frac{Z}{1.1461\times10^{20}})^{\frac{2}{7.3872}}+1]^{\frac{1}{2}}\right\} \tag{3.10}$$

$$Z=\dot{\varepsilon}\exp(\frac{44610.5)}{RT}) \tag{3.11}$$

3.3 Establishment of peocessing map of GH5188 superalloy

From the introduction of Part 2, it can be seen that in the process of thermal deformation of metal materials, the proportional relationship between the energy consumed by tissue deformation and the total energy consumed by deformation can be expressed by the energy dissipation rate η, The expression for the value of η is as follows:

$$\eta = \frac{J}{J_{max}} = \frac{2m}{m+1} \qquad (3.12)$$

During the compression process of the material, when the load reaches a certain critical value, the phenomenon of plastic instability will occur.Prasad proposes a criterion for judging plastic instability based on the principle of maximum entropy generation rate:

$$\xi(\dot{\varepsilon}) = \frac{\partial \ln[m/(m+1)]}{\partial \ln\dot{\varepsilon}} + m < 0 \qquad (3.13)$$

Based on the hot compression test data, the peak stress values at different deformation temperatures and strain rates were read out.Calculate the respective values of η and $\xi(\dot{\varepsilon})$ by formulas (3.12) and (3.13), take the strain rate as the Y value and the temperature as the X value, and use the Origin software to form a matrix, The calculated power dissipation factor as a function of temperature and strain rate is plotted as power dissipation.When $\xi(\dot{\varepsilon})$ is less than 0, it means that plastic instability may occur under this deformation parameter, and this range should be avoided when selecting processing parameters.By superimposing the power dissipation diagram and the plastic instability diagram of each strain value correspondingly, the thermal processing diagrams of 0.2, 0.4, 0.6 and 0.7 strain values can be obtained, as shown in the figure below.

Take the data with a strain of 0.7 as an example for analysis. Figures 3.11(a) and (b) show power dissipation diagrams and plastic instability diagrams.It can be seen from Figure 3.11(a) that when the strain is 0.7, the dissipation rate factor is generally higher in the temperature range of 1160 °C ~ 1180 °C, up to 0.30, indicating that it has a higher deformation rate at high deformation temperature. Good organizational evolution behavior. However, with the change of strain rate,

the value fluctuates greatly, and the η value has two peak areas, which proves that the microstructure evolution behavior of GH5188 superalloy has a great relationship with the strain rate.It can be seen from Figure 3.11(b) that the rheological instability region is mainly concentrated in the high strain rate region. In the region where the strain rate is 0.1s-1~1s-1 and the deformation conditions of the processing temperature are 1080℃~1180℃, the values are all greater than 0, and the minimum value is 0.073, indicating that the processing parameters are well selected. As shown in Figure 3.12, the colored area ξ<0 indicates that this area is the parameter range of rheological instability during thermal deformation of the alloy, and the rheological instability factors in other areas are all positive values, which belong to the safe processing area.
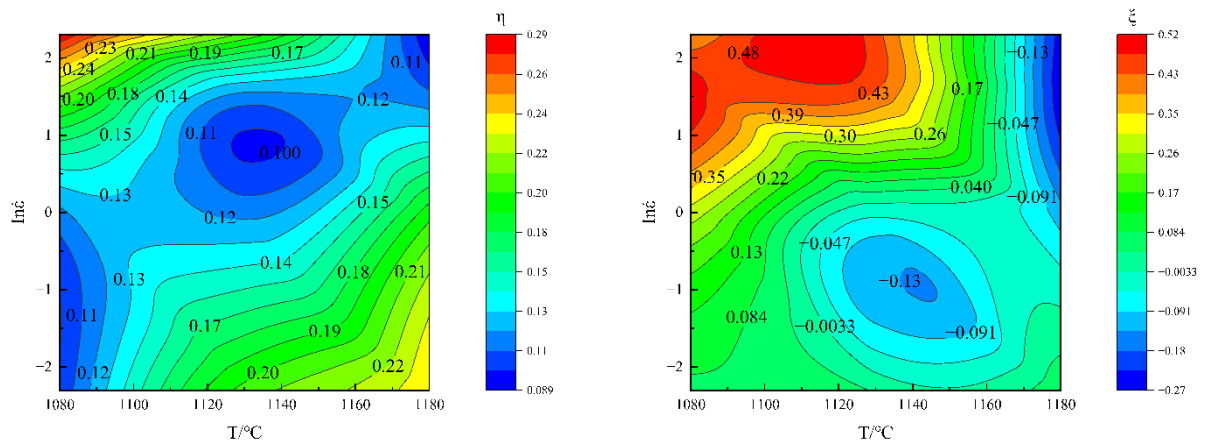

Fig 3.8 - Power dissipation diagram (a) and plastic instability diagram (b) of GH5188 at a strain of **0.2**
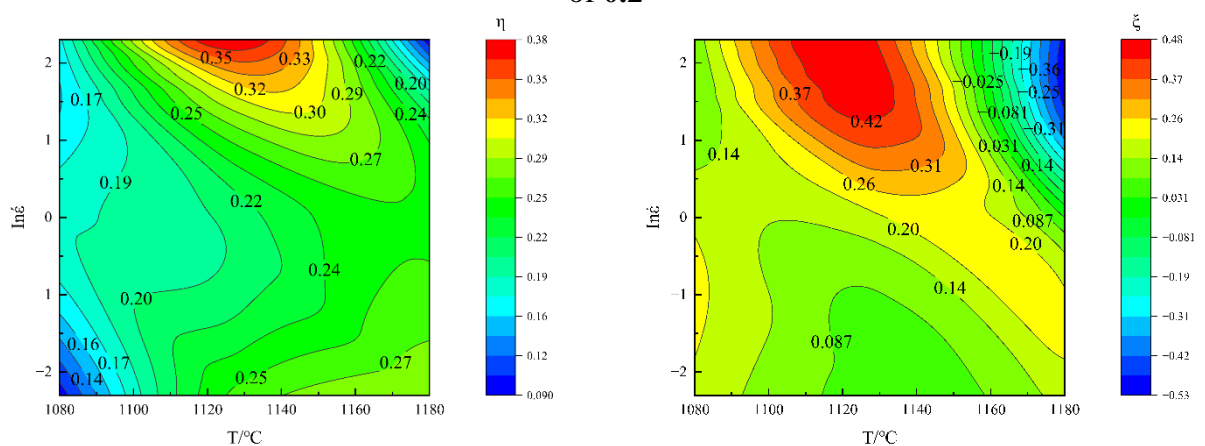

Fig 3.9 - Power dissipation diagram (a) and plastic instability diagram (b) of GH5188 at a strain of **0.4**
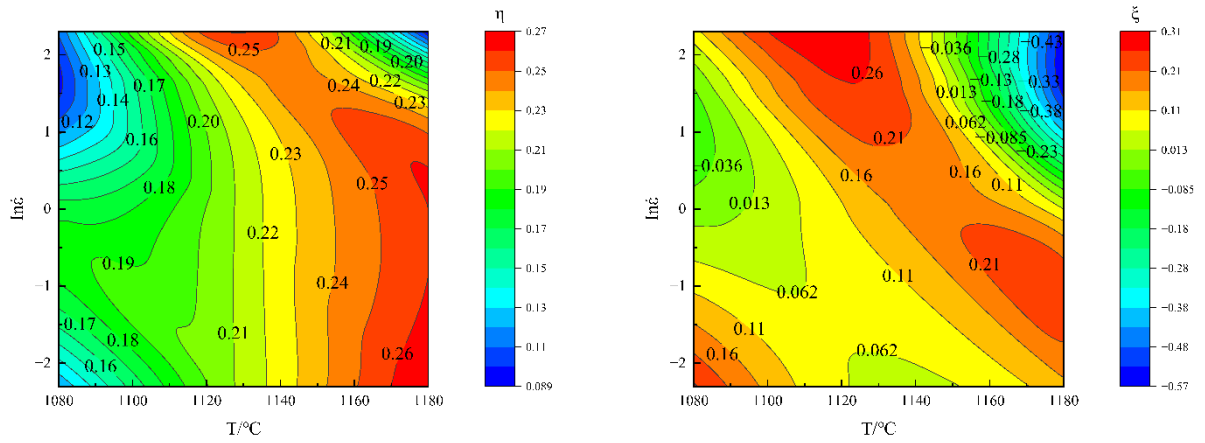
44

Fig 3.10 - Power dissipation diagram (a) and plastic instability diagram (b) of GH5188 at a strain of **0.6**
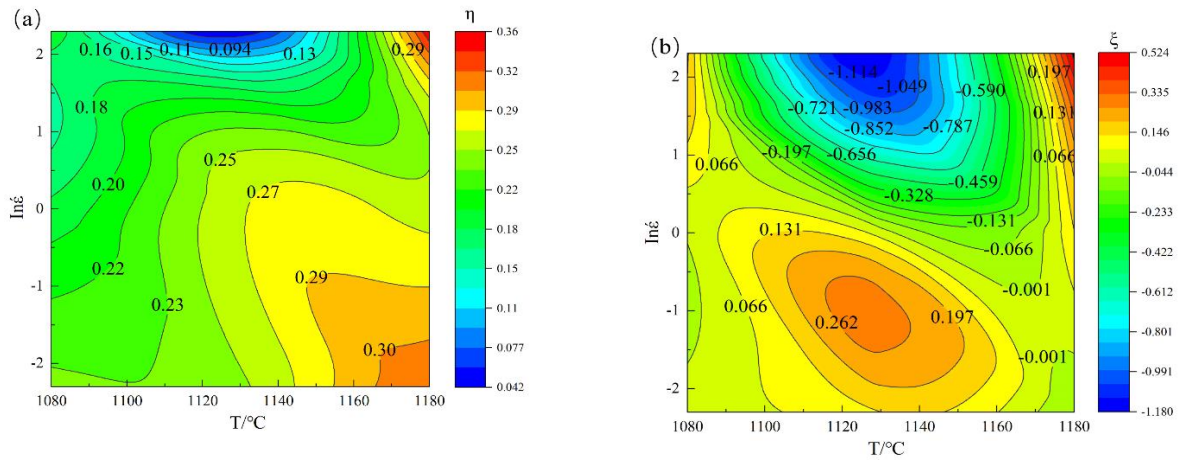

Fig 3.11 - Power dissipation diagram (a) and plastic instability diagram (b) of GH5188 at a strain of 0.6
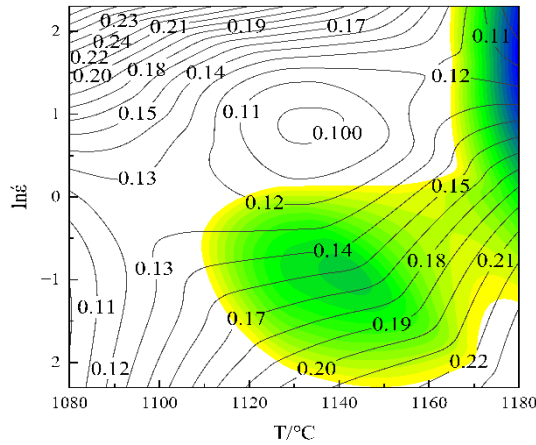

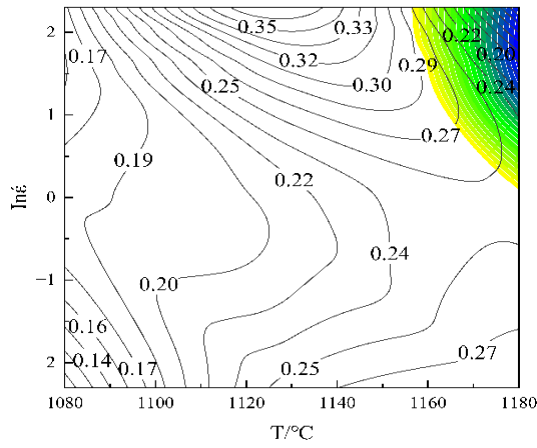Fig 3.12 - Processing map at a strain of 0.2

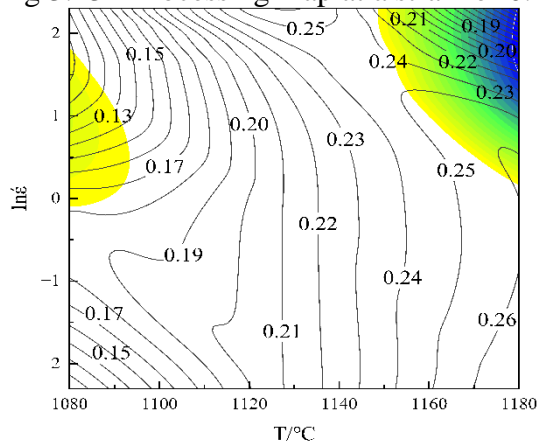Fig 3.13 - Processing map at a strain of 0.4

Fig 3.13 - Processing map at a strain of 0.6
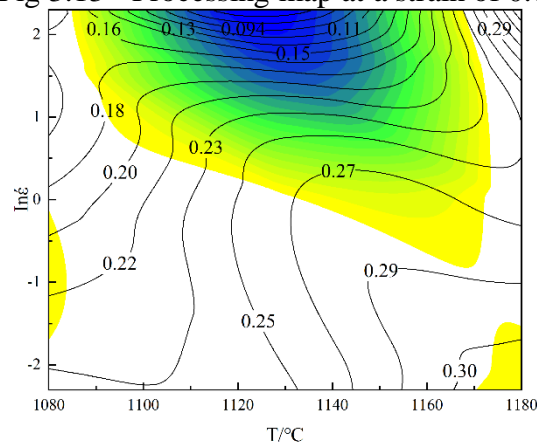
Fig 3.14 - Processing map at a strain of 0.7

It can be seen from Figure 3.15 that when the strain is 0.7, there are three rheological instability regions, which are ： T=1080°C~1090°C ， $\dot{\varepsilon}$=0.14s^{-1}~1s^{-1};T=1090°C~1170°C ， $\dot{\varepsilon}$=0.37s^{-1}~10s^{-1}; T=1170°C~1180°C ， $\dot{\varepsilon}$=0.1s^{-1}~0.22s^{-1}.GH5188 alloy is not suitable for hot working within these three process parameters. At T=1080°C~1180°C, the regional tissue dissipation rate in the range of $\dot{\varepsilon}$=0.1s^{-1}~1s^{-1} is higher, reaching 0.29, while the plastic instability rate is lower and all positive. Therefore, this area is the optimum range of process parameters

46

for GH5188 alloy hot forming. In general, at lower strain rates, the tissue dissipation rate is higher and the plastic instability rate is lower; by reducing the strain rate, the plastic instability region on the graph can be avoided, and a better plastic deformation mechanism can be obtained. For example, when the deformation temperature is about 1130 °C and the strain rate is less than 1s-1, the energy dissipation rate of the microstructure evolution is about 0.25, indicating that the deformation microstructure evolution is more sufficient at this time.Processing within this range is not easy to produce defects such as surface wrinkling and coarse grains, and the material processing performance is good.
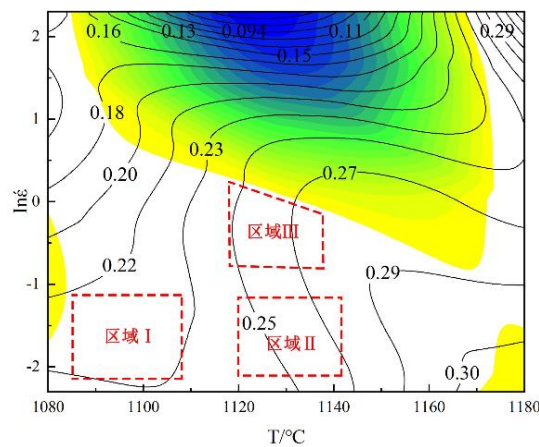
Fig.3.15 - Processing map of GH5188 superalloy at strain of 0.7

The recrystallized grain distribution of the GH5188 compression deformation specimen after thermal compression at a strain of 0.7, different strain rates ($0.1s^{-1}$ and $1s^{-1}$), and different deformation temperatures (1080°C and 1130°C), as shown in Figure 3.16. Figure 3.16 shows the three areas in the thermal processing map that meet the processing conditions:(a) is Domain I (1080°C, $0.1s^{-1}$),(b) is Domain II (1130°C, $0.1s^{-1}$),(c) is the recrystallization distribution diagram of Domain III (1130°C, $1s^{-1}$). By setting the sub-grain boundary judgment standard angle θ_c and the grain boundary judgment angle θ_{GB} in the Channel software, and comparing with the average orientation difference θ_0 in each grain measured by the system, different grain structures can be distinguished.According to the literature [65], the critical orientation difference between the subgrain boundary and the grain

boundary can be set to 2° and 10°, that is, θc=2°, θ$_{GB}$=10°.When the orientation difference is less than 2°, the grains are defined as recrystallized grains, which are indicated in red;The sub-grain is represented by yellow, and the misorientation ranges from 2° to 10°;Deformed grains are defined when the misorientation is greater than 10° and are shown in blue.

Domain I: It can be seen from Fig. 3.16 (a) that the microstructure of the deformed specimen is composed of large-sized work-hardened grains and dynamically recrystallized grains. The size of the grains is uneven, the proportion of fine recrystallized grains is low, the distribution of grains has a large divergence range, and some small-sized grains are distributed on the grain boundaries of the large-sized initial grains. The necklace structure in Figure 3.16(a) shows that the growth of recrystallization is not complete at lower temperatures. It is worth noting that recrystallization nucleation is also distributed on the twin boundaries, accompanied by the bowing phenomenon of the grain boundaries, and small-angle grain boundaries are distributed inside the original grains.Figure 3.17(a) is a histogram obtained by measuring the orientation difference from the center of the grain to the grain boundary along the L1 direction.As can be seen from Figure 3.17(a), the misorientation increases sharply near the grain boundary,It is indicated that the accumulation of a large number of dislocations [66] here leads to the accumulation of dislocations, so that a certain segment in the grain boundary bows out to the side with high dislocation density. Distortion-free recrystallized nuclei are formed. As shown in the box in Fig. 3.16(a), some new grains are rotated after the formation, causing the flat and continuous twin boundaries to be twisted and broken. It can be seen that the dynamic recrystallization of GH5188 is mainly carried out by discontinuous dynamic recrystallization (DDRX) at a temperature of 1080 °C and a strain rate of 0.1 s^{-1}. At the grain boundary and the twin boundary, nucleation is formed in the form of grain boundary bowing, and the growth and rotation of the grain are realized by the movement of the large-angle grain boundary.

Domain II: As can be seen from Figure 3.16(b), compared with Figure 3.16(a),

the size of the grains tends to be concentrated, and the microstructure tends to be uniform.Figure 3.17(b) shows the change in orientation difference along the L2 direction within the subgrain.From Figure 3.17(b), it can be found that the orientation difference curve in the grain fluctuates in a curve shape, and the maximum orientation difference is significantly lower than that in Figure 3.17(a). According to Yu et al. [67], this phenomenon is related to the micro-ribbon structure inside the grains. Due to the alternating orientations in these band structures, the misorientation in the grains gradually decreases, and no accumulation occurs on the grain boundaries.This indicates that during the hot compression of GH5188 superalloy, the intersecting twins achieve grain segmentation and induce recrystallization behavior, that is, twinning-induced continuous dynamic recrystallization (DDRX) mechanism [68].

Domain III: It can be seen from Fig. 3.16(c) that a uniform and fine structure is effectively obtained during hot deformation under this condition, indicating that the recrystallization fraction increases with the increase of the strain rate.The grain information obtained by CHANNEL 5 software is shown in Figure 3.17(d). It can be seen from Fig. 3.17(d) that the recrystallized fraction at a strain rate of $1s^{-1}$ is higher than that at a strain rate of $0.1s^{-1}$. This is due to the rapid increase in the deformation energy storage within the grains at higher strain rates, and the continuous recrystallization with a faster recrystallization rate when the energy is higher than the twinning nucleation energy.And the observation of the microstructure shows that the grains are fine and uniform and all are equiaxed.It shows that the temperature is 1130°C and the strain rate is $1s^{-1}$ is the best processing area of the material.
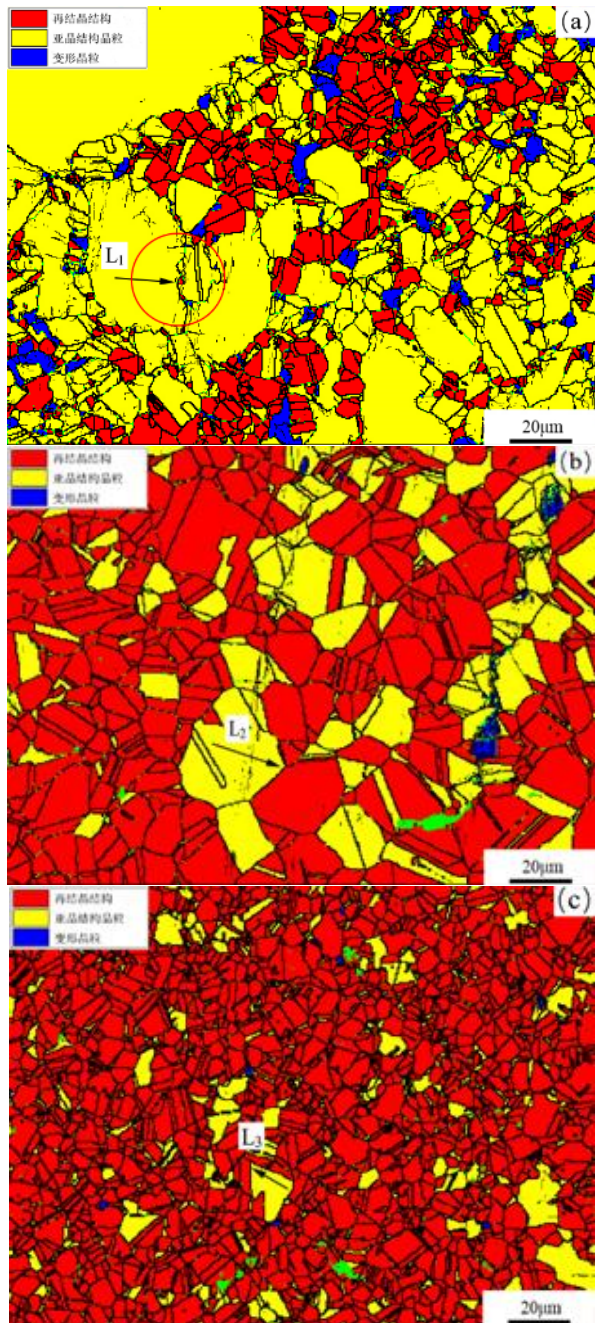
Fig.3.16 - Recrystallized grains of GH5188 at different deformation temperatures, (a) 1080℃, 0.1 s⁻¹ (b) 1130℃, 0.1s⁻¹ (c) 1130℃, 1s⁻¹
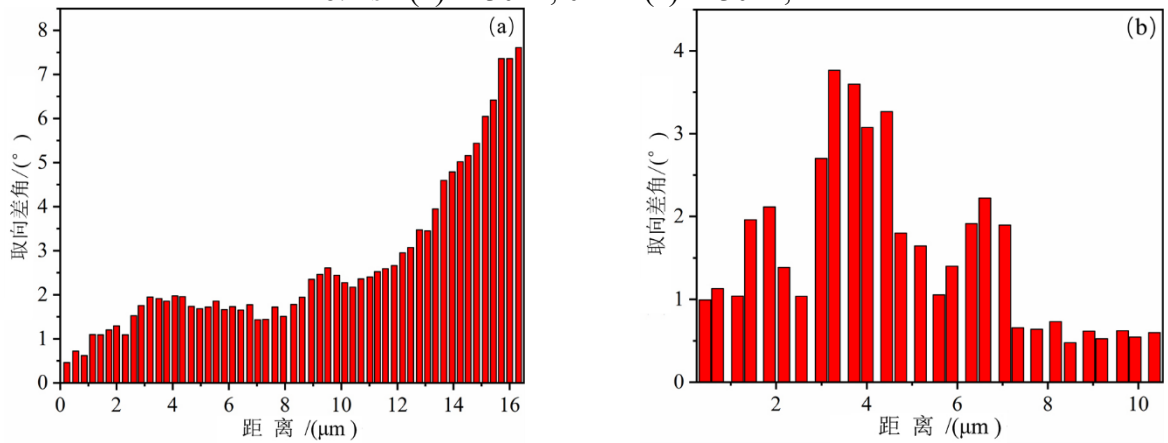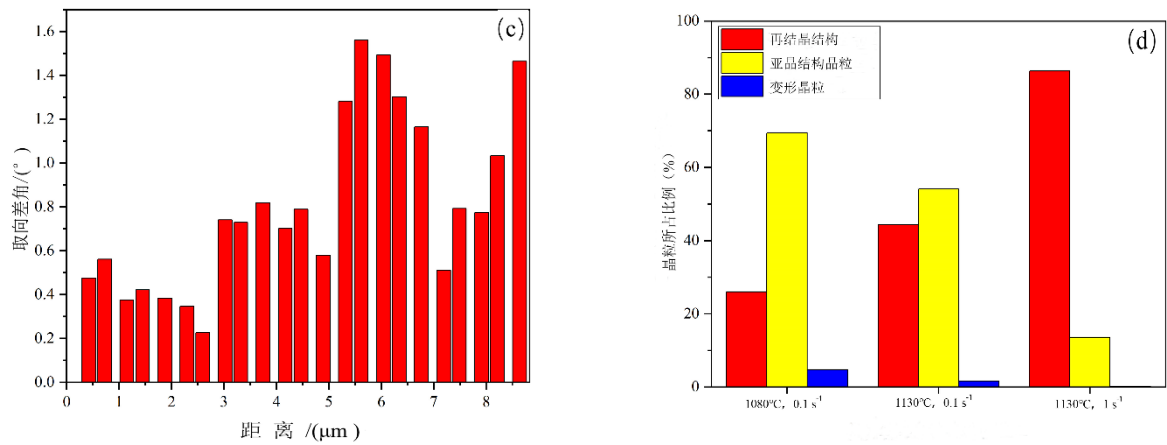
Fig.3.17 - Histogram of absolute misorientation along the line in recrystallized grains at different temperatures, (a) Histogram of L1 misorientation (b) Histogram of L2 misorientation (c) Histogram of L3 misorientation (d) Grain recrystallization ratio graph

3.4 Conclusion:

(1) Based on DMM, the thermal processing map of GH5188 was established.Under the condition that the deformation temperature is about 1130°C and the strain rate is $1s^{-1}$, the energy dissipation rate of GH5188 is about 0.27, which is the safe processing area of the alloy.

(2) By EBSD technique, it was found that the dynamic recrystallization of GH5188 alloy proceeded in a discontinuous recrystallization manner at lower temperature, and the recrystallization fraction of GH5188 increased with the increase of deformation temperature and strain rate.And the recrystallization mode is changed, and it occurs in the form of continuous dynamic recrystallization of twin crystals.When the strain is 0.7, the deformation temperature range is about 1130°C, and the strain rate is about $1s^{-1}$, which is the best deformation parameter of GH5188.

PART4 LABOR PROTECTION

-4.1 Harmful and hazardous working factors

The labor environment of the forging workshop is worse than that of the common machining workshop. The main problems are the poor labor environment, many negative factors and high accident rate in the forging workshop.

4.1.1 Strong vibration.

The vibration of the forging shop mainly comes from the forging equipment [70]. Long-term work in an environment with high vibration intensity will cause psychological and physical diseases, and in severe cases, it will lead to vomiting, dizziness and central nervous system disorders, and reduce work efficiency [71].

4.1.2 High noise.

The noise in the forging workshop comes from various mechanical equipment, such as forging presses, blowers, ventilators and gas heating furnaces. The degree of harm depends on the noise level, frequency and the length of stay in the noise environment. According to the statistics of the International Organization for Standardization, when the noise is 65, 90, 95, 100 dB(A), the incidence of noise-induced deafness after 40 years of work is 10%, 21%, 29% and 41% [72].According to relevant regulations in China, the noise of the forging workshop should be less than 90dB(A), but the noise level in the forging and heating work area generally reaches 97~123dB(A).High noise can cause noise-induced deafness, resulting in mild or moderate hearing loss, and can also induce diseases of the nervous, endocrine and cardiovascular systems.

4.1.3 Poor temperature conditions.

In the hot summer, the temperature of the heating work area exceeds 55°C.Long-term high temperature work can easily cause heat stroke, and also affect the functions of the digestive system and urinary system. In the cold winter, the temperature difference between the work workshop and the external environment can easily cause colds and wind chills. Under the stimulation of hot and cold, the balance between human physiological activities and the outside world

is easily destroyed, which affects the nervous system and reduces the work efficiency of workers.

4.1.4 The problem of thermal radiation.

The forging process requires a high temperature forging furnace to soften the forgings and billets [73]. These furnaces and hot forgings emit harmful rays such as ultraviolet and infrared rays. The thermal radiation of gas heating furnace or oil furnace is as high as 180mW/mm^2, which is easy to damage the human body, especially the eyes, which can cause acute electro-optic eye or dermatitis [74].

4.1.5 Poor air quality.

The air in the forging workshop contains a variety of harmful gases, such as coal gas or lubricant flue gas, dust, heat treatment quenching flue gas, and sulfuric acid or hydrochloric acid gas generated by pickling, which fill the entire workshop.This is seriously irritating to the human respiratory tract and can easily cause diseases; at the same time, when working for a long time, it will inhale too much carbon monoxide gas, which can make some tissues and cells hypoxia, and even endanger life.

4.2 Analysis of working conditions and development of protective measures

In order to ensure the safety and health of workers in the forging process of the clamp, and improve the working environment of workers. Come up with some solutions in terms of regulations and work environment. First, in terms of scientific management, labor protection regulations, systems and technical management standards should be strictly implemented and improved, and the on-site management and management supervision should be scientific. At the same time, the management should attach great importance to the improvement of the working conditions of the forging workshop, carry out the necessary technical transformation of the forging workshop, and incorporate the improvement of labor protection conditions into the reform of the enterprise.

In terms of technical transformation, high-efficiency precision forging and low-polluting crank hot die forging presses or electro-hydraulic hammers with vibration

elimination, energy saving and less pollution can be used to replace the existing steam-air hammers, which can solve the problems of vibration and air quality [75]. And in terms of safety technology, in order to prevent casualties in the labor process and ensure the safety of their lives, corresponding safety technical measures should be formulated according to the different characteristics of different forging workshops. When new equipment is used, safety technical requirements must be met. Before trial production and production, there must be reliable safety measures. And strict requirements are imposed on the working conditions of workers, such as prohibiting fatigue work and drinking work. Secondly, occupational disease inspections for workers should be carried out on a regular basis and should be institutionalized [76].

Make necessary investment in training that is conducive to the health of employees, improve the overall quality of workers, and improve the treatment of blacksmiths. Through the means of technological transformation, the development and use of high-efficiency, energy-saving and safe forging equipment will enable the forging machinery to develop in the direction of mechatronics and the intelligentization of auxiliary systems.

4. 3 Conclusion

For the forging worker, labor protection must be strengthened and the labor environment must be improved. Prevention first, safety first, and the combination of safety technology and system management must effectively protect the work safety of workers.

PART 5. ENVIRONMENTAL PROTECTION

In the machining industry, forging is the one with the greatest impact on the environment, if it is not paid attention to and controlled. The forging plant will pose a great threat to the surrounding air and water sources. Therefore, in order to reduce the environmental problems caused by the forging process, this part mainly describes the content related to environmental protection in the forging workshop.

5.1 Typical environmental problems in the forging process

5.1.1 The problem of wastewater generated in the forging process

As a typical example of thermal processing, forging processing uses a large amount of water, so a lot of waste water will be generated during the forging process. The water used in the forging process is mainly divided into two categories [77]: one is recycled, which basically does not cause pollution or harm to the environment. Another type of production wastewater is discharged to the outside, which will cause different degrees of pollution and harm to the surrounding environment, such as acid or alkaline wastewater discharged during pickling and cleaning of forgings; and cooling water used in the heating furnace; Wastewater discharged from wet dust removal; Oily waste water flowing out from various mechanical equipment or pipeline valves due to leakage; waste water containing various components in the process of cleaning equipment, etc.

5.1.2 Air problems during forging process

Because the burning of fuel in the forging workshop will emit a large amount of toxic gas and soot into the atmosphere; at the same time, the aerosol aerosol that lubricates the mold and the burning of the lubricant will produce toxic gases such as S0, CO, HS, etc; Dust particles when the compressed air blows the mold: Bar cutting and forging cleaning will generate dust; The pickling process may produce steam escape of corrosive acid, etc., and in the forging process, there is inevitable use of steam and compressed air ventilation equipment, which makes the diffusion of dust more serious. And because most of them are close-range operations and are

close to air pollution sources, operators are deeply affected and become one of the occupational diseases of forging.

5.2 Recommendations and measures for treating sewage in forging processing

In the surface treatment process of forgings, in order to eliminate the oxidized part of the surface of the workpiece, for forgings with complex shapes and easy deformation, such as slender rods and thin-walled forgings;For die forgings with high technical requirements, the pickling process is often used [78].According to different forging materials, different pickling media are used, carbon steel and low alloy steel forgings and billets are pickled with sulfuric acid or hydrochloric acid;High-alloy steel and non-ferrous metals are pickled with a variety of acid mixed solutions or acid-alkali compound pickling.Due to the pickling process, acid-containing wastewater is produced.

5.2.1 Acid-containing wastewater

Regarding acid-containing wastewater [79], it can be treated as follows:

① Pickling wastewater to remove oxide skin and impurities, after purification treatment, add new sulfuric acid or hydrochloric acid, and after reaching the required concentration, it is reused for production to realize recycling.

② Waste acid recovery, concentrate acid-containing waste water and send it to waste acid treatment station, and use vacuum evaporation method or combustion heating method to recover acid.

② After the acid-containing wastewater is purified and concentrated, it is sent to the sewage treatment station to use the neutralization method to neutralize the acid wastewater with ammonia water. In this process, sulfuric acid in wastewater is converted into ammonium sulfate, and hydrochloric acid is converted into ammonium chloride, which can be used as agricultural fertilizer.

③ The acid-containing wastewater is treated with limestone, and the acid-containing wastewater is sent to the limestone filter, so that the acid wastewater is neutralized and discharged after reaching the standard.

5.2.2 Oily wastewater

Wastewater containing oil mainly comes from various hydraulic equipment (such as hydraulic presses, hydraulic presses), oil circuit systems used as power pipelines (such as oil pipelines for fuel furnaces), equipment maintenance, cleaning, and mold lubrication. Due to the low reliability of the current hydraulic components, the leakage of oily wastewater is aggravated. Among them, oil is the most common type of oil in oily wastewater [80].

Oily wastewater can take the following measures:

①Hydraulic equipment and pipeline systems, valves and pipelines should be sealed and reliable, and the maintenance of equipment and pipeline systems should be strengthened to reduce leakage.

②Set oil collecting pit or oil collecting device at the lowest position of hydraulic equipment and equipment using lubricant.

③Emulsion wastewater should be set up with an independent treatment system. Air flotation, electric flotation, coagulation sedimentation, etc. can be used.

④ The lubricant for lubricating the mold should be the lubricant with less pollution, and the amount of lubricant and cleaning agent should be reduced as much as possible during the operation.

⑤ Set up an oil collecting pit outside the workshop to centrally treat the oily wastewater in the workshop, and use the gravity separation method to coarse-grain or flotation method to remove heavy oil and floating oil, and discharge after reaching the standard.

5.3 Solutions and suggestions for air pollution problems in the forging process

5.3.1 Combustion waste gas and its treatment

At present, in the forging industry, the use of electric heating technology is rare. In some enterprises, gas or oil is used as fuel, but most small and medium-sized forging workshops use coal as fuel. Coal combustion is the main pollution source of the working space atmosphere [81].

The following measures can be taken to deal with soot-type pollution:

① Where conditions permit, establish gas generating stations to realize central heating, and change the decentralized and independent coal burning method, which is convenient for centralized management.

②Improve the furnace structure, improve the coal feeding method, and make the coal burn as fully as possible.

③ Install smoke and dust removal devices. Select the appropriate dust collector according to the flue gas temperature, composition, dust concentration, and processing air volume.

④The heating furnace shall be equipped with a chimney that meets the requirements, and the combustion exhaust gas shall be discharged into the atmosphere at a certain height outside the workshop, and the flue gas shall not be directly discharged in the workshop.

5.3.2 Waste gas treatment in pickling room

When the forgings are pickled, acid-containing waste gas will be generated in the pickling room. This kind of waste gas not only pollutes the air, but also corrodes the plant, equipment, and endangers the health of operators. For the treatment of acid-containing waste gas, the pickling room is arranged on the downwind side of the perennial wind direction, and it is recommended to build it separately; an extraction hood is installed above the pickling tank, and an acid mist treatment device is installed[82].

5.4 Conclusion

This part mainly describes the current situation of environmental pollution in the forging workshop, and proposes corresponding practical control measures for the existing environmental pollution problems, involving all pollution sources of the forging workshop (factory), such as waste water, waste gas and so on. It is hoped that it will help and improve the environmental protection work in the forging industry.

CONLIUSION

This paper mainly studies the thermoplastic behavior of GH5188 deformed cobalt-based superalloy and the forging process of aviation pipeline clamps.The macroscopic mechanical behavior and microstructure evolution mechanism of GH5188 superalloy were systematically studied by means of thermal deformation physical simulation technology and EBSD analysis technology.Based on the experimental data, the quantitative relationship between flow stress, process parameters and microstructure was established;The nucleation and growth mechanism of dynamic recrystallization and sub-dynamic recrystallization of GH5188 superalloy was studied in depth;

(1) The hot deformation constitutive equation of GH5188 superalloy is obtained:

$$\dot{\varepsilon}=1.1461\times10^{20}\left[\sinh(0.0034\sigma)\right]^{7.3872}\exp\frac{\left[-44610.5\right]}{RT} \qquad (4\text{-}1)$$

$$\sigma=(\frac{1}{0.0034})\ln\left\{(\frac{Z}{1.1461\times10^{20}})^{\frac{1}{7.3872}}+[(\frac{Z}{1.1461\times10^{20}})^{\frac{2}{7.3872}}+1]^{\frac{1}{2}}\right\} \qquad (4\text{-}2)$$

$$Z=\dot{\varepsilon}\exp(\frac{44610.5)}{RT}) \qquad (4\text{-}3)$$

（2）Based on the dynamic material model, the thermal processing diagram of GH5188 superalloy under the processing conditions of deformation temperature between 1080 and 1180 °C and strain rate range of 0.01 to 10 s-1 was established.To avoid rheological instability, processing at low temperatures and low strain rates should be avoided.The optimal process parameters of GH5188 forging are analyzed: when the strain is 0.7, the deformation temperature range is about 1130℃, and the strain rate is about 1s^{-1}

（3）The microstructure is characterized by EBSD technology, and it can be concluded that the GH5188 superalloy undergoes discontinuous recrystallization at a lower energy state; With the increase of energy, it transforms into the way of continuous dynamic recrystallization in twin form. According to the size of the

grain structure, a dynamic recrystallization microstructure evolution model is established.

(4) For the forging worker, labor protection must be strengthened and the labor environment must be improved. Prevention first, safety first, and the combination of safety technology and system management must effectively protect the work safety of workers. for the existing environmental pollution problems, involving all pollution sources of the forging workshop (factory), such as waste water, waste gas and so on. It is hoped that it will help and improve the environmental protection work in the forging industry.

REFERENCES

1. Li Jiarong, Xiong Jichun, Tang Dingzhong, et al. Advanced High Temperature Structural Materials and Technology (Part 1) [M]. Beijing: National Defense Industry Press, 2012:3-4.

2. Yu Yuhong, Sun Kuiping, Deng Xiuqin, et al. Constant temperature oxidation behavior of three iron-nickel-cobalt-based superalloys [J]. Special Steel, 2008(05):35-37..

3. Deng Chao. Structural analysis and optimization design of high temperature and high pressure clamp type quick opening [D]. Beijing University of Chemical Technology, 2017.

4. Zhang Zonghua, Wang Zongwu, Zhang Zhe, et al. Analysis of the standard system of high temperature and high pressure conduit connection clamps [J]. Aviation Standardization and Quality, 2014(06):7-10.

5. Liu Tao, Li Jun. Research and enlightenment on typical standards of foreign aviation high-temperature pipeline connection clamps [J]. Science and Technology Innovation Herald, 2014, 11(05):64-67

6. Zheng Min, Cao Qikai, Sui Fucheng, et al. Research on the connecting clamp of aviation duct [J]. Aircraft Design, 2009, 29(06):57-62.

7. Zheng Min, Zhang Yining, Jing Lulu, et al. Analysis of new foreign fixed clamps with pads [J]. Aviation Standardization and Quality, 2009(05) 12-16.

8. Yin Zeyong, Chen Yanong, Finite Element Calculation and Experimental Measurement of Clamp Stiffness [J]. Journal of Aerodynamics, 1999,14(02):179-182.

9. Zeng Weidong, Zhou Yigang, Zhou Jun, Yu Hanqing, Zhang Xuemin, Xu Bin. Research progress of machining graph theory [J]. Rare Metal Materials and Engineering, 2006,35(5): 673-677.

10. PRASAD Y, GEGEL H L, DORAIVELUS M, et al. Modeling of dynamic material behavior in hot deformation: Forging of Ti-6242[J]. Metallurgical Transactions A, 1984, 15(10): 1883-1892.

11. MEDEIROS S C, PRASAD Y, FRAZIER W G, et al. Microstructural modeling of meta-dynamic recrystallization in hot working of IN718 superalloy[J], Materials Science and Engineering: A, 2000, 293(1–2): 198-207.

12. Srinivasan R, Ramnarayan V, Deshpande U, et al. Computer simulation of the forging of fine grain IN-718 alloy [J]. Metallurgical Transactions A, 1993, 24(9): 2061-2069.

13. Weis M, Mataya M, Thompson S, et al. The hot deformation behavior of an as-cast alloy 718 ingot [J]. Alloy 718—Metallurgy and Applications, 1989, 135-154.

14. Zhou Jiming, Qi Lehua, Chen Guoding. A review of modeling methods of metal constitutive relation in hot forming[J]. Mechanical Science and Technology, 2005(02):212-216.

15. Weis M, Mataya M, Thompson S, et al. The hot deformation behavior of an as-cast alloy 718 ingot [J]. Alloy 718—Metallurgy and Applications, 1989, 135-154.

16. Peng. Microstructure evolution and mechanical behavior of Inconel718 alloy thick plate during hot working [D]. Harbin; Harbin Institute of Technology, 2012: 35-41

17. Huang Qianyao, Li Hankang, et al. Superalloys [M]. Beijing: Metallurgical Industry Press, 2000: 3-4.

18. Guo Jianting. Materials Science of Superalloys: (Part 1) [M]. Beijing: Science Press, 2008:7-10

19. Gui Weimin. Carbide evolution and related properties of cobalt-based superalloys [D]. University of Science and Technology of China, 2017.1-2Sellars C M, Mctegart W J. On the mechanism of hot deformation [J]. Acta Metallurgica, 1966, 14(9):1136-1138.

20. Wang Tao, Min Xiaonan, Li Zhao, Wan Zhipeng, Tan Qianhui, Zhao Zhanglong. Prediction of dynamic recrystallization during hot deformation of GH4049 superalloy[J]. Chinese Journal of Plastics Engineering,

2020,27(07):64-71.

21. Wang Yan, Gu Yu, Wang Jue, Li Jidong.Hot deformation behavior of as-cast nickel-based superalloy GH4698[J].Forging Technology,2021,46(11):250-254.

22. Jiang He, Li Yaojun, Liu Qiyuan, Dong Jianxin.Effect of final forging temperature on hot deformation behavior of GH4738 superalloy[J].Rare Metal Materialsand gineering,2021,50(07):2552-2556.

23. F. Wilhelm, E. Affeldt, E. Fleischmann, U. Glatzel, J. Hammer, Modeling of the deformation behavior of single crystalline Nickel-based superalloys under thermal mechanical loading, International Journal of Fatigue, Volume 97, 2017, Pages 1-8, ISSN 0142-1123.

24. Abdallah Shokry, Samer Gowid, Sabry S. Youssef, Modeling the flow behavior of Haynes 214 superalloy during hot deformation using mathematical and artificial intelligence-based models, Materials Today Communications, Volume 33, 2022, 104326, ISSN 2352-4928.

25. Ren Xin, Dou Chunyue, Gao Zhiyu, Zhuang Da, Qi Pengtao, He Wei. Research progress of numerical simulation technology of heat treatment[J].Materials Review,2021,35(19):19186-19194.

26. Qiu Qian, Wang Cru, Lu Shiqiang, Ouyang Delai, Li Xin, Zhang Kaiming, Gao Xin. Numerical simulation of thermal compression instability deformation of SP700 titanium alloy [J]. Rare Metal Materials and Engineering, 2022,51(08) :2985-2991.

27. Jiang,R, Proprentner D, Reed PA S.Role of oxygen in enhanced fatigue crackingin a PM Ni-based superalloy: Stress assisted grain boundary oxidation or dynamicembrittlment[J]. Corrosion science, 2018,139: 141-154.,

28. Jiang,R,Pierron F,Reed P A S. Characterisation of strain localisation processesduring fatigue crack initiation and early crack propagation by SEM-DIC in anadvanced disc alloy[J]. Materials Science and Engineering A,2017,699:128-144.

29. China Machinery Industry Federation. Mechanical Properties Test [M].

Beijing: Machinery Industry Press, 2001

30. Wang Wenbin.Research on high temperature deformation behavior of 800H alloy based on hot compression simulation experiment[J].Foundry Technology,2014,35(07):1387-1389.

31. Saeed Aliakbari Sani, Hossein Arabi, Gholam Reza Ebrahimi,Hot deformation behavior and DRX mechanism in a γ-γ/ cobalt-based superalloy,Materials Science and Engineering: A,Volume 764,2019,138165,ISSN 0921-5093,

32. Frost H J,F.Ashby M. Deformation-mechanism maps: the plasticity and creep of metals and ceramics [M]. Pergamon Press,1982: 265-276.

33. Raj R. Development of a processing map for use in warm-forming and hot-forming processes [J]. Met allurgical Transactions A,1981,12(6):1089-1097.

34. Prasad Y,Gegel H, Doraivelu S, et al. Modeling of dynamic material behavior inhot deformation: forging of Ti-6242[J]. Metallurgical Transactions A,1984,15(10):1883-1892.

35. Huang Youlin, Wang Jianbo, Ling Xueshi, et al. Research progress of thermal processing map theory [J. Materials Review: Nano and New Materials Special, 2008, 3: 173-176..

36. Prasad Y V. Author's reply: Dynamic materials model: Basis and principles [J].Met allurgical and Materials Transactions A, 1996,27(1): 235-236.

37. Prasad Y,Seshacharyulu T. Modelling of hot deformation for microstructuralcontrol [J]. International Materials Reviews,1998,43(6): 243-258.

38. Gegel H L,Malas J,Doraivelu S, et al. Modeling techniques used in forgingprocess design [J].ASM Handbook,1988,14:417-438.

39. Malas J C, Seetharaman V. Using material behavior models to develop processcontrol strategies [J].JOM,1992,44(6): 8-13.

40. Alex ander J,Lenard J. Modelling of hot deformation of steels [M]. Berlin:Spr inger Verlag,1989: 105-115.

41. Yu Xiaolu, Li Fuguo, Li Miaoquan. General constitutive equation and its

optimization for thixomorphic deformation of semi-solid materials [J]. Chinese Journal of Mechanical Engineering, 2007, 43(10):72-76.

42. Lei Jinwen, Xue Xiangyi, Zhang Siyuan, Ren Yong, Wang Kaixuan, Xin Shewei, Li Qian. High-precision thermal deformation constitutive model of Ti6242s alloy based on artificial neural network[J].Rare Metal Materials and Engineering,2021,50(06): 2025-2032.

43. Hee-Soo Kim, Si-Jun Park, Seong-Moon Seo, Young-Soo Yoo, Hi-Won Jeong, HeeJin Jang, Regression analysis of high-temperature oxidation of Ni-based superalloys using artificial neural network, Corrosion Science, Volume 180, 2021, 109207, ISSN 0010-938X.

44. Osman Palavar, Dursun Özyürek, Ali Kalyon, Artificial neural network prediction of aging effects on the wear behavior of IN706 superalloy, Materials & Design, Volume 82, 2015, Pages 164-172, ISSN 0264-1275.

45. Sun Chaoyang, Huang Jie, Guo Ning, Yang Jing.Study on physical constitutive model of Fe-22Mn-0.6C type TWIP steel based on dislocation density[J].Acta Metals Sinica,2014,50(09):1115-1122 .

46. Su Jing, Guo Weiguo, He Kexin, Li Yuzhuo.Plastic flow characteristics of AZ31 cast magnesium alloy and constitutive relation of physical concepts[J].Chinese Journal of Nonferrous Metals,2011,21(01):44-50.1004.0609.2011. 01.003.

47. Wang Jun, Wang Cru, Lu Shiqiang, Li Xin, Ouyang Delai, Qiu Qian, Gao Xin, Zhang Kaiming. Strain-compensated physical constitutive model of NiTi shape memory alloy[J]. Journal of Materials Heat Treatment, 2022,43(01): 184-188.

48. Cai J, Wang K, Zhai P, et al. A Modified Johnson-Cook Constitutive Equation to Predict Hot Deformation Behavior of Ti-6Al-4V Alloy[J]. Journal of Materials Engineering and Performance, 2015, 24(1): 32-44.

49. Liu Shaofei, Qu Yinhu, Wang Chonglou, et al. Research progress on constitutive models of metals and alloys during high temperature deformation [J]. Materials Review, 2018, 32(7): 2241-2251.

50. Deng Xuefeng, Zhang Hui, Chen Zhenhua. Constitutive equation of heat-resistant aluminum alloy (FVS0812) sheet under warm tension [J]. Chinese Journal of Plastic Engineering, 2006, 13(3): 83-87.

51. Lin Y C，Ding Y，Chen M S.et al. A new phenomenological consti-tutive model for hot tensile deformation behaviors of a typical Al-Cu-Mg alloy[J].Materials and Design,2013,52(12);118.

52. Zhou Jiming, Qi Lehua. Research on the rheological constitutive equation of AlsO3s/LY12 composites under hot compression[J]. Chinese Journal of Plastic Engineering, 2005, 12(5): 58-62

53. Wang Ruining. A thermal deformation constitutive model of titanium matrix composites [J]. Thermal Processing Technology, 2009, 38(42): 65-67

54. Li Wei. Effects of strain rate and temperature on mechanical properties of composite TP-650[J]. Rare Metal Materials and Engineering, 2010,39(7):1195-1198..

55. Liu Manmen. Reactive Synthesis of Ag/SnO: Finite Element Simulation of Composite Extrusion Process [D]. Kunming University of Science and Technology, 2008. He Yusong. Study on high temperature tensile deformation and fracture behavior of spray-deposited 7075A1/SiCp composite plate[D]. Hunan University, 2007.

56. Li Hongjie. Research on the mechanical properties of nano-AlzO3 particles reinforced aluminum matrix composites [D]. North University of China, 2011.

57. Jonas J J, Sellars C M, Tegart W J M. Strength and structure under hot-working conditions[J]. Metall Rev, 1969, 14(1):1-24.

58. Zener C, Hollomon J H. Effect of strain Rate Upon Plastic Flow of steel [J]. Journal of Applied Physics, 1944, 15(1):22-32.

59. N. D. Ryan，H.J. McQueen. Comparison of dynamic softening in 301，304,316 and 317stainless steels. High Temp Tech.1990,8:185-200.

60. Xu Yangtao, Wang Yonghong, Ma Hongli.Research status of tensile and compressive deformation mechanism of cobalt and cobalt-based

alloys[J].Materials Review,2020,34(19):19117-19121.

61. Edited by the editorial committee of "China Aviation Materials Manual". China Aviation Materials Manual [M]. Beijing: China Standard Press, 2002, 07.

62. Prasad Y, Gegel H L, Doraivelus M, et al. Modeling of dynamic material behavior in hot deformation: Forging of Ti-6242 [J]. Metallurgical Transactions A, 1984, 15(10):1883-1892.

63. Prasad Y, Seshacharyulu T. Modelling of hot deformation for microstructural control [J]. International Materials Reviews, 1998, 43(6): 243-258.

64. Li Sha, Zeng Li, Miao Huajun, et al. Hot deformation behavior and thermal processing diagram of nickel-based superalloy GH4700[J]. Journal of Materials Heat Treatment, 2013, 34(9): 51-56

65. Jorge-Badiola D, Iza-Mendia A, Gutiérrez I. Evaluation of intragranular misorientation parameters measured by EBSD in a hot worked austenitic stainless steel[J]. Journal of Microscopy, 2007, 228(3) : 373-383．

66. CUI Z Q, QIN Y C. Metallography and Heat Treatment [M], Beijing: Machinery Industry Press, 2007: 194-210.

67. YU C, DI H S, ZHANG J Q, et al. An electron backscattered diffraction study on the dynamic recrystallization behavior of a nickel–chromium alloy (800H) during hot deformation[J]. Materials science and Engineering A, 2013, 585(15): 71-85.

68. ZHOU G. Study on high temperature deformation behavior and deformation mechanism of nickel-based superalloys [D]. Northeastern University, 2013: 150-152.

69. State Machinery Industry Commission. Primary Forging & Stamping Technology [M]. Beijing: China Machine Press, 1988-12:11-12

70. Wang Zhigang, Fan Lixia. Analysis of Workpiece Rotating Vibration in Radial Forging Process [J]. Forging & Stamping Technology,2011,36(02):5-9.

71. Xiao Yuan. Examples of European Union's Efforts to Reduce Tool Vibration Damage [J]. Power Tools,2016(03):28-30.

72. Guo Yutong. Study on the Psychological Effect and Cognitive Performance of Aviation Maintenance Noise [D]. Civil Aviation Flight College of China,2022.

73. Sheng Y. Study on effects of high temperature thermal radiation on physiological indexes and tolerance of human body [D]. Tianjin: Tianjin University.2008. (in Chinese)

74. Huang Pu Hao. Influence of Outdoor Thermal Environment Factors on Human thermal comfort [D]. Central South University.2014

75. Wang Hanqing (Ed.). Ventilation Engineering [M]. Beijing, China Machine Press, 2006.

76. LD/T 71.10-2009, Forging processing labor quota of rail transit Equipment Manufacturing Industry [S].

77. Lei Zhongbin. Analysis of environmental factors in forging workshops and countermeasures for labor protection [J]. China Molybdenum Industry, 2000(04):50-55.

78. Wei Yunhan. Case of Cold Rolling Acid-Alkali Wastewater Treatment Reconstruction Project [J]. Water Purification Technology, 2022, 41(S1): 193-196

79. Wang Yunfei, Dong Jinji. Optimization and improvement of cold rolling acid-base wastewater treatment process [J]. Metallurgical Power, 2020(01):50-51

80. Ma Dexu. Treatment technology of acid-containing and oil-containing wastewater from stainless steel cold rolling [J]. Environment and Development, 2017, 29(09): 87-88

81. Xu Shaochun.Research on pollution control of heavy oil combustion exhaust gas[J].Railway Occupational Safety, Health and Environmental Protection, 1998(04):13-17

82. Liu Qijue. A measure of waste gas treatment in pickling workshop [J].

Journal of Wuhan Institute of Food Industry, 1997(03):65-67.